To be updated.

Julian Austin

Department of Mathematics, Statistics and Physics.
Newcastle University

This dissertation is submitted for the degree of
Doctor of Philosophy

April 2021

Dedication will be here.

Declaration

Declaration to be placed here.

Julian Austin
April 2021

Acknowledgements

Acknowledgements to be place here.

Abstract

Abstract will be written here.

Table of contents

List of figures

List of tables

Nomenclature

Roman Symbols

J_i	Number of temporal observations for i^{th} functional observation.
N	Number of spatial observations.
$\mathcal{S}$	Spatial Domain.
$\mathcal{T}$	Temporal Domain.
t	Temporal dimension.
$\mathcal{X}$	Functional random variable.
y_{ij}	Observed response at time t_j for i^{th} functional observation. See Equation 1.2.
Y	Observed data set. See Equation 1.1.

Greek Symbols

χ	Functional data (observation of $\mathcal{X}$).
ε_{ij}	Noise process at time t_j for i^{th} functional observation. See Equation 1.2.

Subscripts

i	Spatial index.
j	Temporal index.

Acronyms / Abbreviations

CESM	Community Earth System Model.
EO	Earth Observation.
FDA	Functional Data Analysis.
$\mathcal{GP}\left(m(\cdot), k(\cdot,\cdot)\right)$	Gaussian Process with mean function $m(\cdot)$ and covariance function $k(\cdot,\cdot)$
NCAR	National Centre for Atmospheric Research.
PS	Pressure at reference height of 2m from CESM-LE, [27]

SAR Synthetic Aperture Radar.

TMQ Total vertically integrated precipitation from CESM-LE, [27]

TREFHT Temperature at reference hieght of 2m from CESM-LE, [27]

U10 Wind speed at height of 10m from CESM-LE, [27]

Chapter 1

Introduction

1.1 Earth observation

Many area of science produce data on both a spatial and temporal scale. Take for example, the production of Earth observation data. Earth Observation (EO) is the collection of information on the state of a physical, chemical or biological system of the planet. Typically EO data is acquired through some form of remote sensing in addition to perhaps some in-situ measurements. Typically EO data is acquired to study a process either over a large area of land, a large time horizon, or both. For example such EO studies include; land usage change in wetland environments in southern Spain, [37], crop production in the Netherlands, [28], and land deformation of the Tuscany region over a two year time period, [41]. In each case there is significant spatial and temporal dependency that is to be considered in the observed processes. For example Raspini et al. use the temporal dependency in ground deformation signals to highlight areas of significant change in movement, [41]. They combine this with spatial maps to provide a monitoring bulletin for their area of interest. Of course to provide actionable insights from EO data requires an understanding of both the spatial and temporal dependency and as such models that can handle both forms of dependency whilst maintaining parsimony are desired in the EO community.

The three studies highlighted above all use space borne remote sensing to observe their process of interest. Space borne remote sensing, typically achieved through the use of satellite based sensors, is becoming more prominent as a source of EO data. This is largely due too the increase in satellites launched which have been designed to capture various processes of the earth. Figure 1.1 highlights the rise in availability of a single type of remote sensing satellite. One particularly prominent remote sensing system is the European Space Agency's Sentinel Constellation, [3]. The Sentinel constellation of satellites provides a wide range of remote sensing sensors which are easily accessible. The constellation provides capabilities capturing various EO processes through various forms of sensors such as Synthetic Aperture Radar (SAR), optical and multispectral sensors. As such the Sentinel constellation has been widely used in EO studies. For example the

three studies above, [37, 28, 41] all utilise the Sentinel 1 SAR sensors for their observation source.

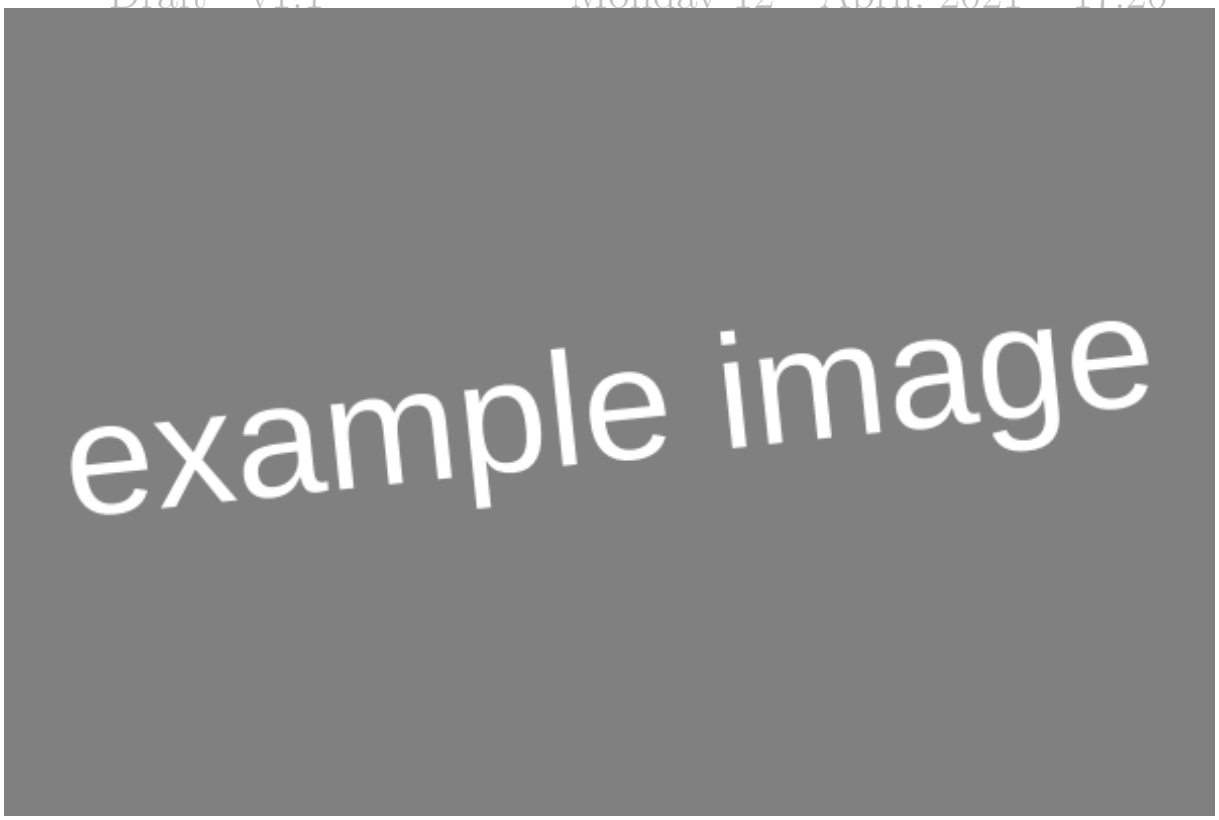

Fig. 1.1 A timeline of major satellite launches and operating periods for EO missions using SAR based sensors.

A prominent focus of the Sentinel satellite constellation is their ability to provide repeated observations at relatively high frequency, [3]. This is in response to the rising demand for monitoring EO processes over time. This has been made possible by the development of remote sensing technologies which makes the revisit time possible. For example the Sentinel 1 satellite constellation can provide revisit times of approximately five days for areas of Europe. Such short revisit times are advantageous as they give higher temporal resolution and thus models can incorporate this additional information. For example, Raspini et al. utilise this in their study of land deformation change to identify anomalous regions. Figure 1.2 gives an example of EO data taken from the Sentinel 1 satellite of the Sentinel constellation. The figure gives an idea about the spatial and temporal resolution available using such a data source. The increasing availability of high temporal frequency EO data such as those provided by the Sentinel satellite constellation thus drives a demand for statistical models which can handle high resolution spatial and high resolution temporal dependency.

Another area where EO data is prominent is climatology. In this setting the focus, rather than in the geological studies in [37, 28, 41], is on the study of the atmosphere and weather over the globe. In this case spatial and temporal dependency in the EO data used in various climatology studied is obvious. For example, consider the Community Earth System Model (CESM), [27], produced by the National Centre for Atmospheric Research

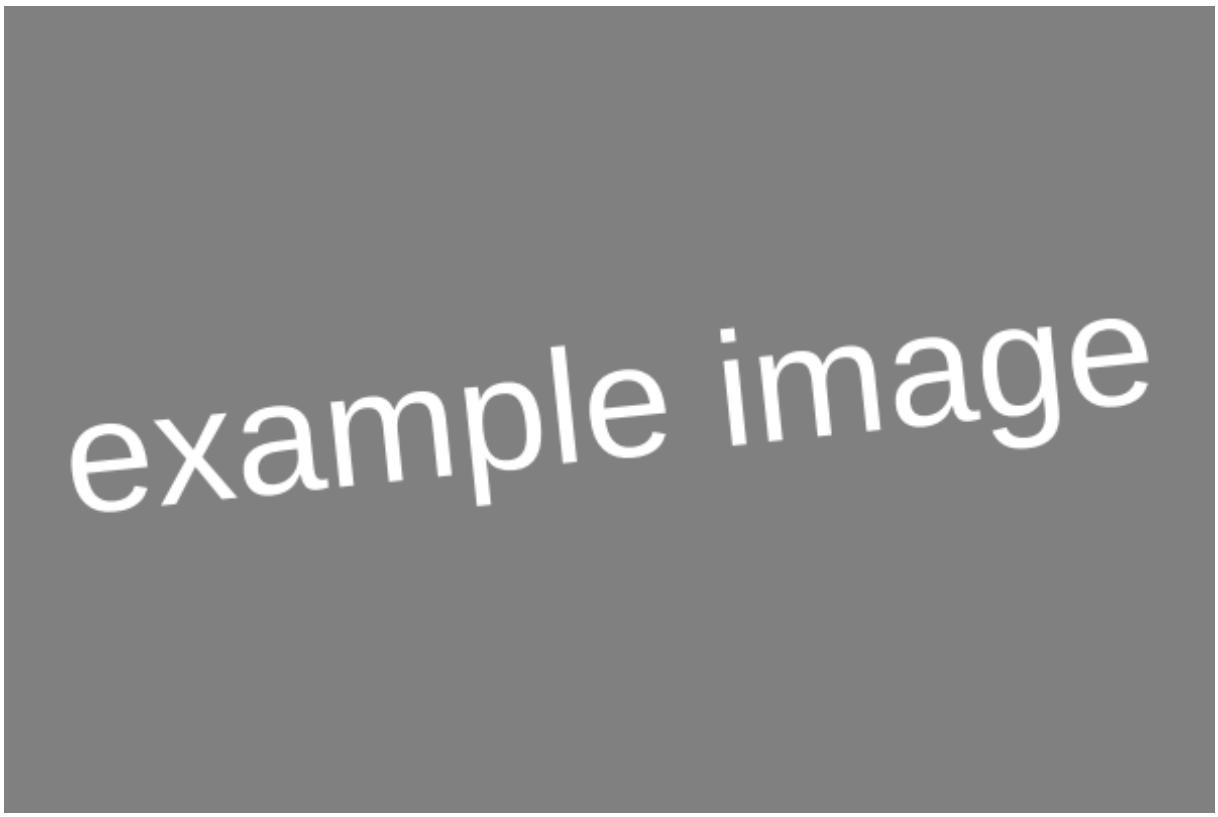

Fig. 1.2 An collection of Sentinel 1 SAR images over Newcastle, UK for the period between January 2019 and January 2021. This example of Earth observation data exhibits spatial and temporal dependencies. Contains modified Copernicus data.

(NCAR). Such a model provides simulations of various aspects of the Earth's climates for past, present and future time points. The data derived through the CESM shares various aspects with typical remotely sensed EO data such as the Sentinel data.

In particular, both sources of data share an inherent spatial and temporal dependency. That is to say the underlying process driving both remotely sensed observations of the Earth and the CESM simulations will vary over the globe and also will be driven by the state of the system at a prior time points. That is not to say the process is the same for both but rather that there is a commonality in that they could both be considered spatio-temporal processes. In addition there are more concrete similarities in the data. Typically, both data sources are described on a lattice of points over space which is usually regular. Such a lattice is usually represented through a geodetic coordinate system which grounds an datum to a real world location. Finally, both sets have repeated observations through time over the same space. Due to the cross over in properties of both data sources typically we observe similar statistical techniques being used for both.

The description of such spatio-temporal processes is well studied in statistics and a large amount of effort has been used to develop various models to suit them. A well known monograph which deals with such processes is that written by Cressie and Wikle, [9]. The monographs details various forms of spatio-temporal processes and typically focuses on the extension of spatial method to incorporate the additional temporal dimension. We discuss these methods in more detail in Section 1.3. Of particular importance is that temporal

and spatial dimensions are distinct as they are inherently different in the physical process. For example one could consider a spatial point influencing its neighbours in all directions however a temporal point reasonably shouldn't influence its past. As such there is often a distinction in the method used to model the temporal and spatial aspects of the physical process.

Another area of statistics which is often used to model data with temporal dependency is Functional Data Analysis (FDA). FDA is typically applied to analyse data which vary over a continuum. Time is one such continuum. EO data with high frequency temporal observations are therefore suitable candidates for FDA models. FDA is a relatively new branch of statistics and as such few studies have been presented which use FDA techniques on EO data. Liu et al. considers FDA techniques on periodic EO data, [31] and similarly Hooker et al. considers FDA techniques to model the Harvard modified vegetation index sourced from EO data. In both the above studies they consider EO data as a collection of functional observations which each observation representing the trajectory of response over time. The monograph of Ramsay and Silverman provides a comprehensive introduction to the themes of FDA, [40]. FDA are often intuitive since viewing responses as being discretely sampled from an unknown smooth random function in some contexts closely matches the actual data generating process compared to a multivariate analysis. Therefore the use of such techniques could be helpful in modelling such high frequency ST data in conjunction with the multivariate methods discussed by Cressie and Wikle in [9]. However, focus in the FDA literature to date has primarily revolved around independently observed functional data. This is typically not the case in our motivating case of Earth observation data where there is often obvious spatial dependency. Thus there is a need to describe functional data models which incorporate dependency among observations. In this work we consider developing such models for dependent functional data with a focus on application to Earth observation data. We consider adapting well studied FDA methodologies and borrow techniques from spatio-temporal statistics to allow for spatially dependent observations. In Section 1.2 we make concrete our definition of functional data.

1.2 Functional representation

As mentioned in 1.1 EO data can be viewed as a collection of functional data. However there is a choice about how we interpret observations in this conversion. We may consider the data as a collection of functional observations with time being our functional dimension and space our collection dimension. Or we may consider the functional observations having a spatial domain and the collection dimension being time. The canonical presentation of functional data in FDA is to use time as the functional dimension, [40] and thus we use the below definition of functional data from this point of view.

1.2.1 Functional data

Multivariate data analysis usually revolves around the study of observations which are finite dimensional and is well studied. Modern data collection techniques can now create data which are extremely numerous and thus can often be viewed as functions and in some sense infinite dimensional.

For example, Ferraty and Vieu consider the case where we can observe a random variable at several times between some minimum and maximum time, $(t_{\min}, t_{\max})$. A single observation can then be considered as the collection $\{X(t_j); j = 1, 2, \ldots, J\}$ where J is the total number of temporal sample points and $X(t)$ is the response variable at time t. Unlike multivariate data we consider the case that the separation between observations becomes minimal. That is we consider the data as an observation from the continuous random process $\mathcal{X} = \{X(t); t \in (t_{\min}, t_{\max})\}$. We therefore propose as in [14] and [46] the following definition of a *functional variable*.

Definition 1.1 (Functional Variable)**.** *A random variable $\mathcal{X}$ is called a functional variable if it takes values in an infinite dimensional space (or functional space). An observation χ of $\mathcal{X}$ is called a functional data.*

Further to this, suppose we observe a collection of functional data (realisations of $\mathcal{X}$). Then we will denote this collection by the term *functional dataset*.

Definition 1.2 (Functional Dataset)**.** *A functional dataset, $\chi_1, \chi_2, \cdots, \chi_N$ is the collection of N realisations of functional variables $\mathcal{X}_1, \cdots, \mathcal{X}_N$ identically distributed to $\mathcal{X}$.*

The canonical way to present functional data and the subsequent methods is to use time as the continuous variable, [40, 14, 46], as described above. However, there is no such restrictions in either Definition 1.1 or Definition 1.2. In fact, another case is to consider the functional domain of the variables to be space. In our proposed methodologies we present when possible with respect to time due to the simplification it brings in notation. We will make explicit reference to when we change the domain of our functional data, for example if we consider space as our continuous domain.

We introduce the following notation for use in the remainder of this work. We consider our EO data set to be observed in some spatial domain which we denote by $\mathcal{S} \subset \mathbb{R}^2$ and temporal domain donated by $\mathcal{T} \subset \mathbb{R}$. Any observed dataset we can enumerate with one index over the spatial location and the other indexing the temporal locations. For completeness we introduce two separate notations, one for the case when we wish to treat time as our domain for the functional variable and the other for treating space as the domain for the functional variable.

We assume our dataset is comprised of N spatial locations and let $\boldsymbol{s}_i \in \mathcal{S}$ be the spatial location of the i^{th} observed functional variable. At each spatial location we suppose we observe J_i temporal observations and denote by $t_{ij} \in \mathcal{T}$ the j^{th} temporal observation of the i^{th} functional variable. Then our dataset can be summarised by Y where:

$$Y = \{y_{ij}; i = 1, 2, \cdots, N, j = 1, 2, \cdots, J_i\} \tag{1.1}$$

where y_{ij} is the response value of the i^{th} functional variable at time t_{ij} observed with error. That is we consider for each spatial location the discrete temporal observations being a sample from a realisation of a functional variable observed with error. That is:

$$y_{ij} = \chi_i(t_{ij}) + \varepsilon_{ij} \tag{1.2}$$

where as in Definition 1.2 χ_i is a realisation of functional variable $\mathcal{X}_i$ for $i = 1, 2, \cdots, N$. We consider each functional variable as being identically distributed as $\mathcal{X}$. As is common in most observation models we assume we observe data with error, typically one assumes that the error process $\{\varepsilon_{ij}; i = 1, 2, \cdots, N, j = 1, 2, \cdots, J_i\}$ is a white noise process with variance σ_ε^2.

In this case one considers the modelling of the EO dataset by ensuring smoothness of some kind over the temporal domain via its functional data representation. We can then consider building in spatial dependency by assuming a sampling correlation in our N functional data. An area where such spatial dependency has been long studied is multivariate spatio-temporal methods we discuss the common method in the following section.

1.3 Spatio-Temporal methods,

In the statistical literature spatial and spatio-temporal models have been extremely well studied, especially due to the prevalence of geo-statistical applications. In the following we briefly review some of the most commonly observed spatial and spatio-temporal statistical models in the multivariate analysis literature.

The monograph of [8] and references within provide a succinct summary of traditional methodologies in spatial statistics, many of which are applicable to remotely sensed data. Generally speaking spatial data can be split into one of three categories; geo-statistical, area and point process data. In this work the EO data described in Section 1.1 are most suitably modelled using geo-statistical models. The canonical model used in geo-statistical setting is the Kriging model. The Kriging model is well described in [47]. Such models treat spatial data as samples from a random spatial process and that predictions for unknown values can be calculated from a weighted combination of known values in a neighbourhood of our unknown location utilising the correlation among neighbouring points. A prime example of the spatial Kriging model in use for remote sensing data is given in [42]. Extensions to the basic Kriging technique have also been employed across a number of geo-statistical settings, including Co-Kriging involving extra covariate information for reconstruction, [58]. Kriging is well known in many fields through various names, in the FDA literature it is most often referred to as Gaussian Processes Regression. Shi and Choi describes in detail the concept of Gaussian processes in the context of functional regression.

As is detailed in [8] an key aspect to geo-statistical modelling is the specification of spatial dependency in the observed data. A common way for such specification is through

parametric covariance or kernel functions. [8] details the traditional stationary parametric functions such as the Matèrn covariance. These commonly rely on the assumption of isotropy and stationarity in modelling which rarely holds in practice. Further literature has considered extensions of these and is in fact an active area of research. Schmidt and Guttorp compares a variety of methods for producing non stationary and heterogeneous covariance structures for the goal of spatial interpolation, [45]. They group the various methods of creating such structures into four categories; deformation, convolution, covariate and stochastic partial differential equations. The deformation approach proposed by Sampson and Guttorp extends the anisotropic stationary covariances such as though describe in [8] by allowing for a non linear transformation to the space which creates a latent space where isotropy holds, [44]. The convolution approach proposed by Higdon uses a specific form of the covariance kernel which can be represented as a convolution between a convolution kernel and a white noise process. We discuss such an approach more in Chapter 5. The covariate based non stationary kernels tends to be constructed using an adaption to the convolution or deformation approaches with specific covariates. Finally the stochastic partial differential equation method proposed by Lindgren et al. construct non stationary covariances as the resultant Gaussian process is the solution of a stochastic partial differential equation and allowing the parameters of the equation to vary over space, [30].

A natural extension to purely spatial modelling of spatio-temporal data is to include the temporal domain that is often present, such models are known as spatio-temporal models. Spatio-temporal models are well discussed the monograph [9]. In addition spatio-temporal Kriging models are well suited to our data however such models are relatively scarce in the literature. [35] considers the application of such modelling in the satellite remote sensing literature and reasons the lack of such modelling is primarily due to the added complexity such models produce in specifying valid and appropriate space-time covariance functions. As such one particular direction spatio-temporal modelling has considers is the creation of spatio-temporal covariance functions. [7, 17, 25] consider the construction of non separable covariance functions in the early literature. Separability between spatial and temporal correlations is often a key assumption in some methods due to the ease on computations involved in such models, as such [36, 15, 4] considers tests for when such assumptions hold. In particular for EO data, [16] consider such selection of separable covariances and [12] consider such models for air pollution data.

1.4 Summary of Research

The motivation of this work is to provide a model designed for EO data which provides an explanation of both the spatial and temporal process in a parsimonious way. We present a novel method named Correlated Principal Analysis through Conditional Expectation (CPACE), that is designed for modelling EO data. The model builds upon existing FDA techniques to extend modelling from independently observed functional data to functional data which exhibits spatial correlation. The emphasis in the work is to utilise the FDA

paradigm over the temporal domain to aid in the decomposition of the data, with the understanding that our data generating process is smooth across the temporal domain. Such a decomposition gives a parsimonious description of the data over the temporal domain into its principal modes of variation. We then estimate a spatial correlation structure for each component using well known spatial statistical methods. The combination of the resulting estimated spatial covariance structures with the principal directions aims to capture the majority of temporal and spatial dependency observed in the data. We can then utilise the CPACE model to help predict response at unseen spatial and temporal locations, which is a keen area of interest in EO studies. We asses our model using various simulated data both with known correct data generating distribution and to simulations drawn from an incorrect data generating procedure. We apply our CPACE model to the select atmospheric variables from the CESM data set as an example application of the model to EO data.

In particular the work is structured as follows. In Chapter 2 we describe our example data sets which we use to illustrate the performance of the model. In Chapter3 we present the methodologies underpinning the CPACE models, these are typically well known FDA and spatio-temporal statistical methods. We also present the smoothing methodologies used to estimate the mean and covariance surfaces of our random functional variables. In Chapter 4 we present an interim model built on the combination of two well known existing methodologies in the FDA literature with a focus on application to an Earth observation data set. Such a model proposes an novel approach to modelling Earth observation data but helps to highlight the need of including both spatial and temporal effects in modelling such data. In addition the proposed model in Chapter 4 provides an opportunity to explore EO data where the functional domain is space rather than time. We present the benefits and limitations of such an approach in practice in this chapter also. In Chapter 5 we introduce the main contribution of this work which is the CPACE model for correlated functional data. We describe the model in details as well as provide asymptotic results for the model. In Chapter 6 we apply the CPACE model to simulated and real world data sets. Simulation results are presented with comparisons to various existing models with a focus on comparative ability to recover known data generating parameters. Applied results to real world data sets are included with comparisons to existing techniques with a focus on interpolation and forecasting abilities of the model. In Chapter 7 we highlight the practical difficulties in implementing the model with discussion on various techniques which are used to overcome the high dimensionality which is typical in the EO data. Finally, in Chapter 8 we draw the conclusions of the work and present area of further work.

Chapter 2

Data sets

In the following chapter we describe in detail our data which we will use as a source for assessing the performance of the models described within. We use a publicly available set of climate model simulations known as the CESM Large Ensemble (CESM-LE) data set, [27]. The CESM-LE data set provides a good example of EO data that is discussed in Section 1.1. This data set will be used throughout this body of work as a intriguing example of the abilities of the discussed methodology.

2.1 Community Earth System Model - Large Ensemble, [27]

The CESM-LE data set is an extremely popular and significant data set in the climate research community. It was developed to enable the assessment of recent past and near future climate change in the presence of internal climate variability, [27]. It does so by providing 40 simulations of a complex climate model where each simulation is subject to the same radiative forcing scenario but begin a slightly perturbed atmospheric state. As such the forty resultant simulations present the various trajectories the model might take due to internal climate variability of the model.

The model used to run the forty member ensemble is the Community System Earth Model version 1, [20], with the Community Atmosphere model version 5, [20], as the atmospheric component. The model is a fully coupled climate model which consists of a model for each the Land, Ocean, Atmosphere and Sea Ice components of the climate. These are brought together with a coupler model. Figure 2.1 provides a simple overview as to how CESM model couples the various components. Such a model is capable of simulating various Land, Ocean, Atmosphere and Sea Ice variables of the climate, such as the wind speed, temperature or pressure. The CESM-LE produces simulations of such variables on the nominal 1 deg horizontal separation across the globe which induces our spatial resolution of the data. The ensemble produces results at varying levels of temporal resolution between the years 1920 and 2100 for non-control simulations. The temporal resolution varies by variable of interest between 6-hourly, Daily, and Monthly frequency of observations.

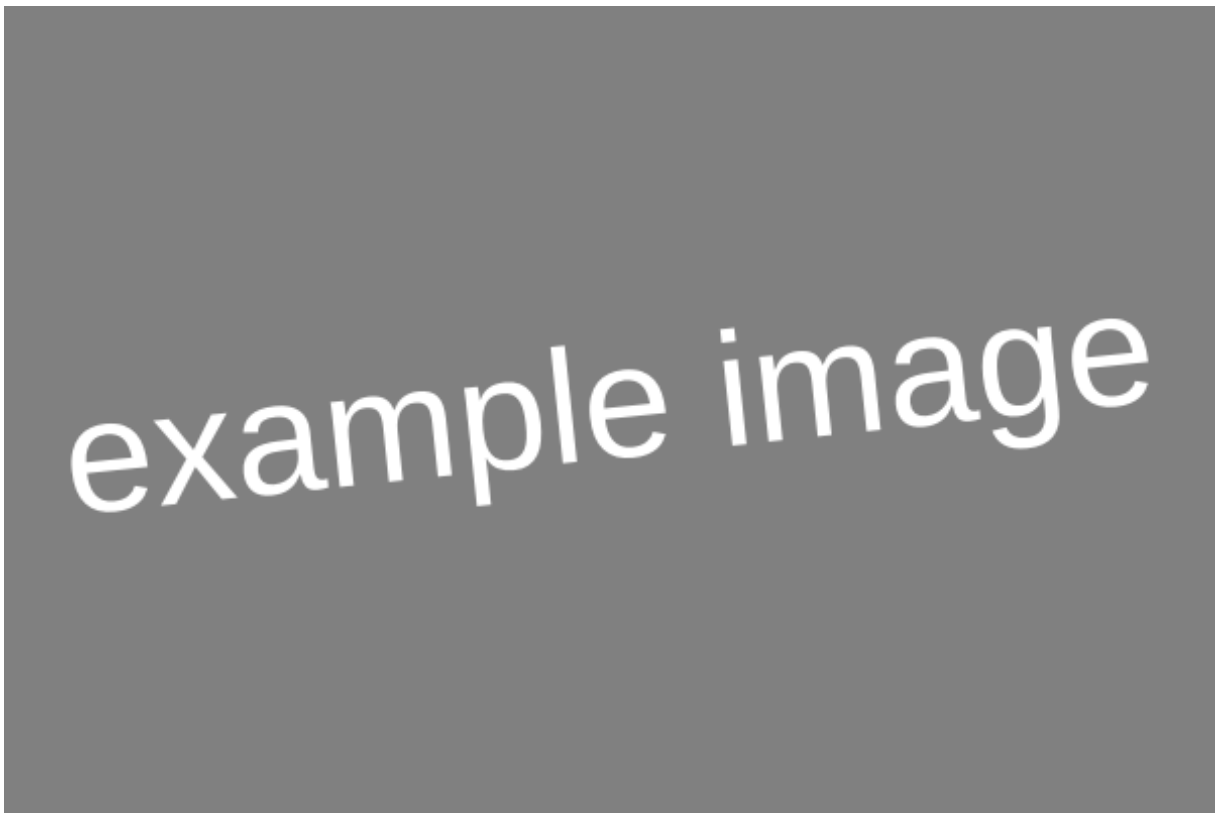

Fig. 2.1 The component models for the full CESM model, [27].

For this body of work we use the CESM-LE data by considering the forty members as separate simulations. Each simulation giving us a realisation of the various climate variables generated by the process described in [27]. We apply a set of preprocessing to the raw data provided by CESM-LE as described below.

2.1.1 Preprocessing

The main preprocessing step we take from the CESM-LE data is to reduce the data size through a series of spatial resampling and temporal cut off. We reduce the data size by considering only a subset of the full data set. We only consider modelling the times between December 2020 and January 2025. These time points were chosen such that the length of time gave reasonable ability to capture periodic elements but that the size of the data did not become too large. By using monthly frequency observations and this 5 year time horizon we have a temporal dimension of 60 for each spatial grid point.

Additionally, to reduce the size of the data further, we resample the model simulations to a smaller spatial grid. Figure 2.2 shows the resampled spatial observation grid over the globe that we use. Resampling is achieved by averaging values of neighbouring pixels until our desired resolution is achieved. In this case we resample until the spatial size of the data set is 64×96 which corresponds to a reduction factor of 3 from the original CESM-LE data. Obviously using such an approach reduces the resolution and thus our ability to see small scale spatial patterns however it allows the data sets to be much more manageable in terms of performing computations over them.

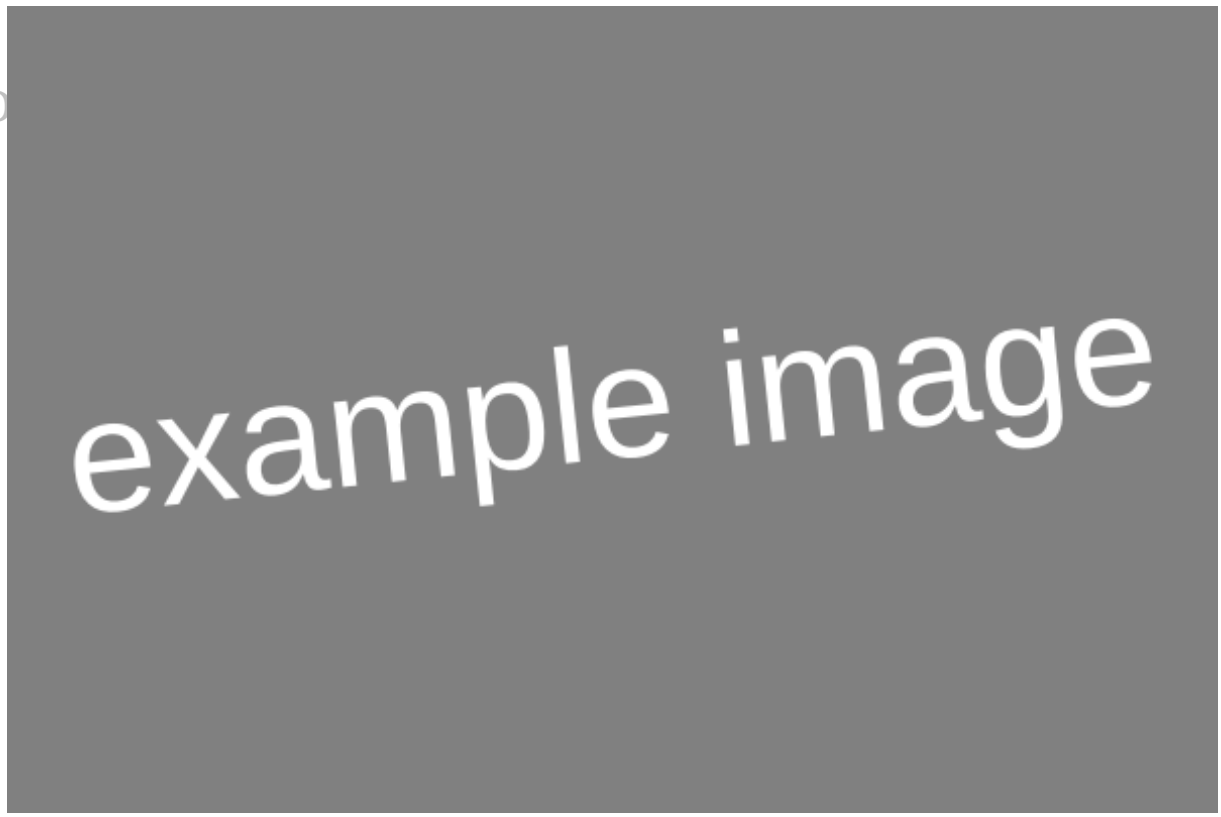

Fig. 2.2 The resampled spatial grid of observation measurements across the globe.

2.1.2 Variables

In the following work we focus on four atmospheric model variables from the CESM-LE simulations. These are; Pressure, Temperature, Precipitation, and Wind. We describe each component in detail in their respective section and throughout this work we consider each as a separate EO data set.

Precipitation

The total (vertically integrated) precipitable water component abbreviated as TMQ in the model descriptions is an atmospheric component output of the CESM-LE. The component is given units of $\mathrm{kg\,m^{-2}}$ and is available monthly on the full spatial grid with monthly precipitation being average over time from the model 6 hourly output.

We can see clearly the spatial variability of the precipitation over the globe by considering the heat map of June 2021 monthly precipitation for a single simulation which is shown in Figure 2.3a. As one would expect there is clear spatial correlation as for example the tropics observe large amounts of precipitation whereas desert regions observe little. We can similarly observe clear temporal correlations in the precipitation variable of the CESM model. In particular Figure 2.3b shows the time series of two locations on the globe. Each exhibit clear periodic signals as wet seasons and dry seasons repeat each year.

JA: Add commentary on the spatial correlation structure and possible non-stationarity.

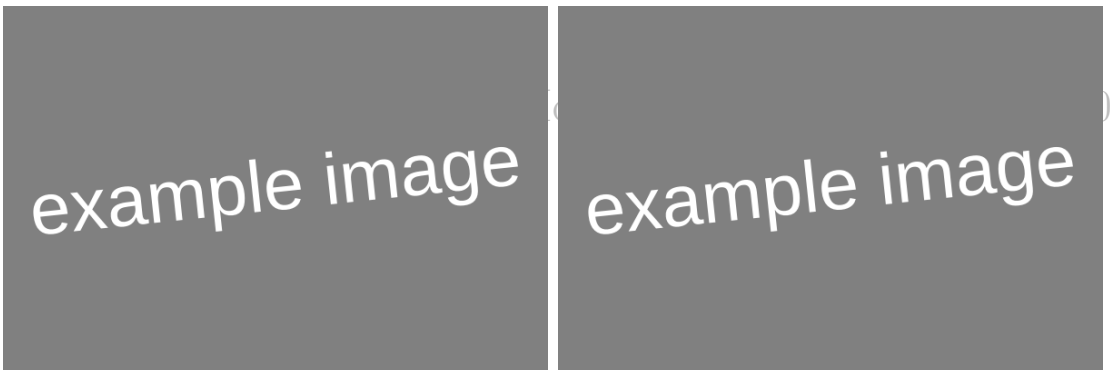

(a) TMQ as at June 2021. (b) TMQ over time.

Fig. 2.3 Overview of the monthly average precipitation variable from CESM-LE ensemble member 1. Figure 2.3a highlights the spatial correlation present while Figure 2.3b highlights the temporal correlation at two distinct locations.

Pressure

The surface pressure component abbreviated as PS in the model descriptions is an atmospheric component output of the CESM-LE. The component is given in units of Pa and is available monthly on the full spatial grid with monthly pressure being averaged over time from the model 6 hourly outputs.

We can see clearly the spatial variability of the pressure over the globe by considering the heat map of June 2021 monthly pressure for a single simulation which is shown in Figure 2.4a. One can clearly see areas of high and low pressure. For example the high pressure zone over the North Atlantic and low pressure zone over Asia. We can similarly observe clear temporal correlations in the pressure variable of the CESM model. In particular Figure 2.4b shows the time series of two locations on the globe. Each exhibit clear smooth signals over time.

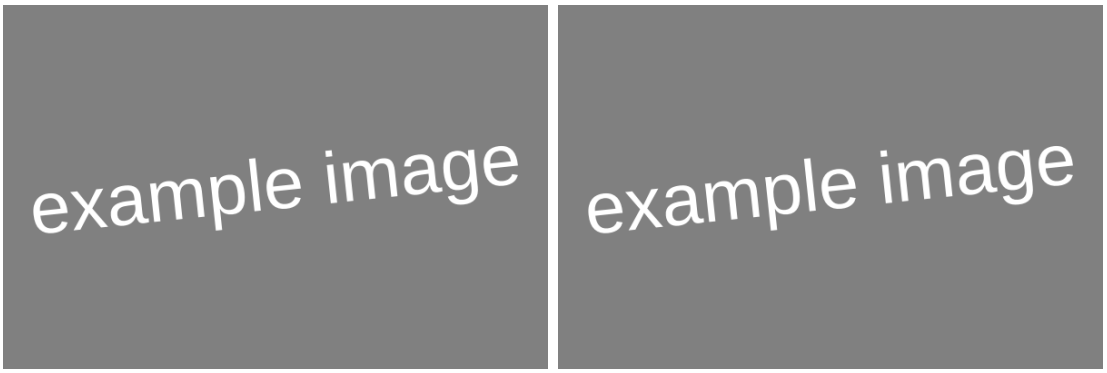

(a) PS as at June 2021. (b) PS over time.

Fig. 2.4 Overview of the monthly average pressure variable from CESM-LE ensemble member 1. Figure 2.4a highlights the spatial correlation present while Figure 2.4b highlights the temporal correlation at two distinct locations.

JA: Add commentary on the spatial correlation structure and possible non-stationarity.

Temperature

The temperature model component abbreviated to TREFHT in the model description is an atmospheric component output of the CESM-LE. The variable refers to the average temperature in K at the model reference height which is 2m above sea level. The average is available monthly with the average being that of the model 6 hourly output for the month. Such a response variable is again available on the full spatial grid of the model.

Quite clearly the temperature exhibits clear spatial correlation across the globe and periodic signals through time as area move from winter to summer. Figures 2.5a, 2.5b highlight this for the spatial and temporal correlation respectively.

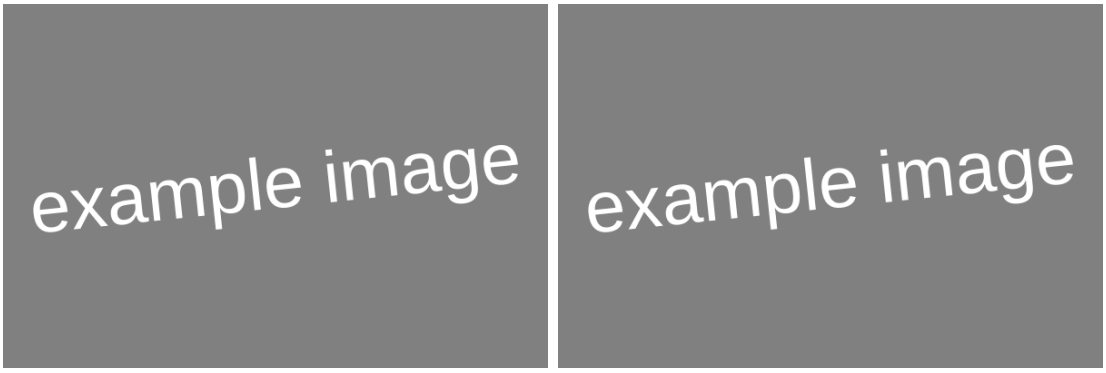

(a) TREFHT as at June 2021. (b) TREFHT over time.

Fig. 2.5 Overview of the monthly average temperature variable from CESM-LE ensemble member 1. Figure 2.5a highlights the spatial correlation present while Figure 2.5b highlights the temporal correlation at two distinct locations.

JA: Add commentary on the spatial correlation structure and possible non-stationarity.

Wind

The wind model component abbreviated to U10 in the model description is an atmospheric component output of the CESM-LE. The component refers to the average wind speed in $\mathrm{m\,s^{-1}}$ at a height of 10m. Again the component is available on the full spatial grid and is available as a monthly average over time.

The wind variable is tightly related to that of the pressure, described in Section 2.1.2, due to the nature of the phenomenon. As such there is clear spatial and temporal correlations in the variable. We visualise the spatial correlation in Figure 2.6a by considering a snap shot of the average wind in June 2021. Comparing such a figure with that of the Pressure variable in Figure 2.4a we can see clear relationship with the two variables where the average wind speed is highest as we move from points of high pressure to those of low. Winds alike the other model variables also exhibit temporal correlation.

JA: Add commentary on the spatial correlation structure and possible non-stationarity.

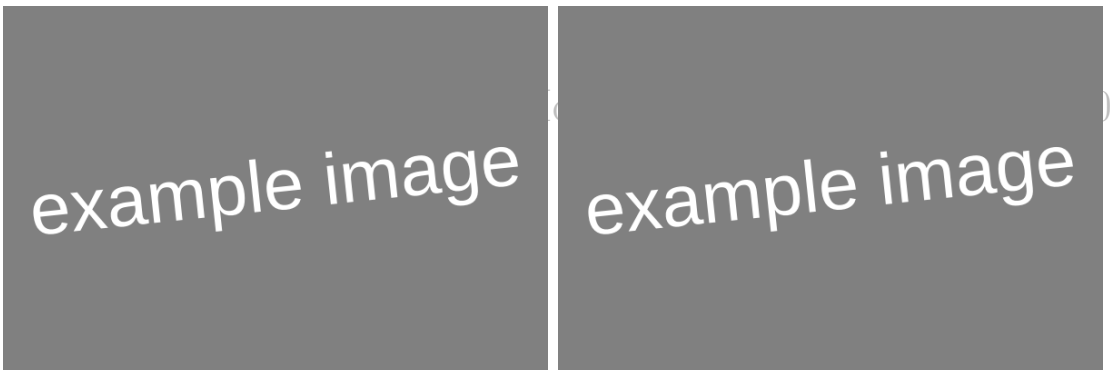

(a) U10 as at June 2021. (b) U10 over time.

Fig. 2.6 Overview of the monthly average wind variable from CESM-LE ensemble member 1. Figure 2.6a highlights the spatial correlation present while Figure 2.6b highlights the temporal correlation at two distinct locations.

2.1.3 Simulations

For each variable discussed in Section 2.1.2 the CESM-LE data provides forty simulations, one from each ensemble member. We have highlighted the variable spatial and temporal correlations in the four variables discussed in the Figures 2.3, 2.4, 2.5, and 2.6 for a single simulation. However we also have variability within simulations and it is useful to view the variability in the variables by the separate realisations of the CESM model. It is important that any model developed for such data should be able to account for this variability in the data generating process. Figure 2.7 displays a snap shot of the standard deviation of the respective variables in June 2021.

JA: To do discussion on areas of increased variability with commentary on how these will probably be the area with most uncertainty in prediction.

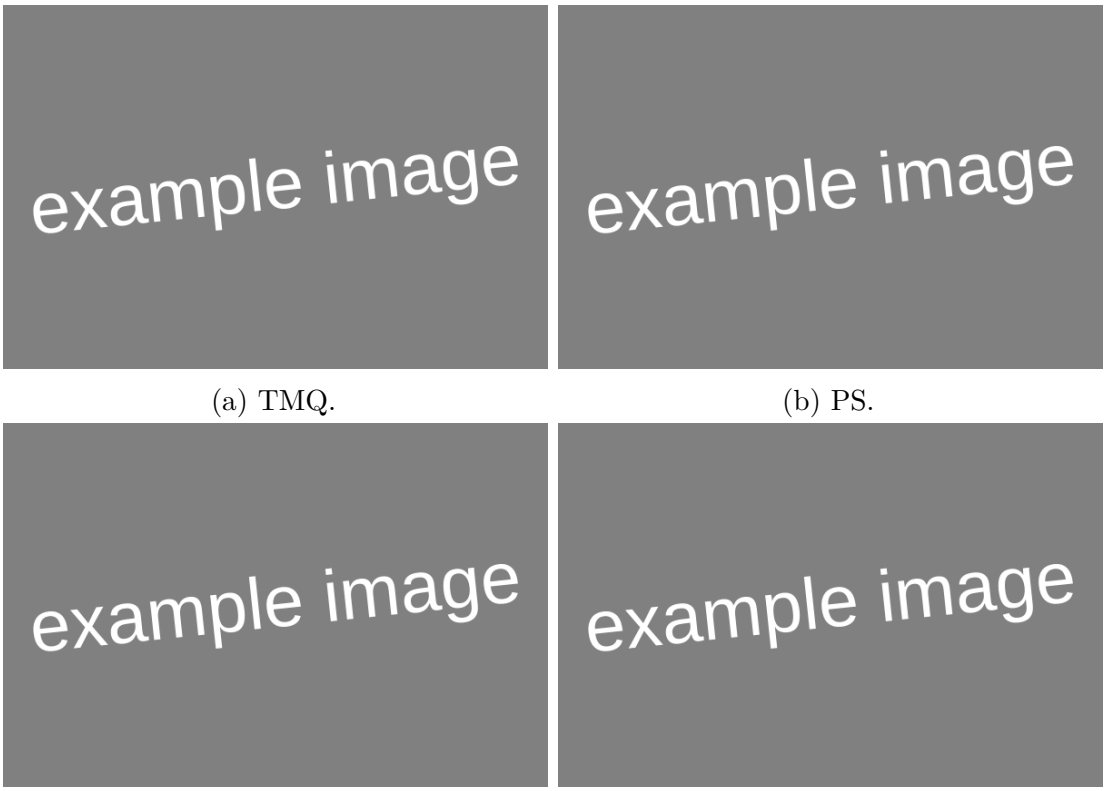

(a) TMQ. (b) PS.

(c) TREFHT. (d) U10.

Fig. 2.7 Standard deviation of the four variables considered at June 2021 for the 40 simulations present in the CESM-LE data set.

Chapter 3

Background Methodologies

In the following chapter we consider the various statistical methodologies upon which we build our CPACE model. This chapter is roughly structured so that we first focus on FDA techniques which are applicable, followed by smoothing methodologies which are use in the FDA techniques. Finally we discuss the multivariate techniques that are used in the CPACE model.

3.1 Functional principal components analysis

A commonly used technique in multivariate statistics is that of Principal Components Analysis (PCA), [52]. The use of such a technique to find dominant directions of variation helps achieve dimensionality reduction and offers a parsimonious way to view data which is driven by the data themselves. The equivalent technique when the data are functional in nature is known as Functional Principal Components Analysis (FPCA). The basic concepts of which were studied in the mid twentieth century. The work of Karhunen and independently Loève paved the basic foundations of the technique in the FDA literature, [26, 32]. The FPCA technique essentially stems from representing the random function $\mathcal{X}(t)$ as an infinite linear combination of orthogonal functions. Such a representation is now known as the Karhunen-Loève theorem after its discoverers.

3.1.1 Formulation

The formulation of FPCA begins by assuming that $\mathcal{X}(t)$, $t \in \mathcal{T}$ is a square integrable stochastic process over some domain $\mathcal{T}$. Let the mean and the covariance of the stochastic process $\mathcal{X}$ be denoted by $\mu(t)$ and $G(s,t)$ respectively, where:

$$\mu(t) = \mathbb{E}(\mathcal{X}(t)) \tag{3.1}$$

$$G(s,t) = \mathrm{Cov}(\mathcal{X}(s), \mathcal{X}(t)) \tag{3.2}$$

Associated with the covariance surface $G(s,t)$ we have the linear operator T_G defined by:

$$T_G : L^2(\mathcal{T}) \to L^2(\mathcal{T}) \tag{3.3}$$

$$T_G : f \mapsto T_G f = \int_{\mathcal{T}} G(s,\cdot)\, f(s) ds \tag{3.4}$$

As T_G is a linear operator we can consider its eigenvalues and eigenfunctions which we will denote by λ_k and ϕ_k respectively (following convention set out in [57]) for $k = 1, 2, \cdots,$. These are defined as the solutions to the Fredholm integral equations of the second kind:

$$\langle G(\cdot,t), \phi_k \rangle = \lambda_k \phi_k(t) \tag{3.5}$$

where $\langle f, g \rangle = \int_{\mathcal{T}} f(s)g(s)ds$ is the inner product in the space $L^2(\mathcal{T})$. Then by the Karhunen-Loève theorem one can express the centred process through the eigenvalues and eigenfunctions of the linear operator associated to the covariance surface. That is:

$$\mathcal{X}(t) - \mu(t) = \sum_{k=1}^{\infty} \xi_k \phi_k(t) \tag{3.6}$$

where ξ_k is the k^{th} principal component associated to the eigenfunction ϕ_k. The Karhunen-Loève theorem assures us this L^2 convergence is uniform in t. The principal components are given by the following:

$$\xi_k = \langle \mathcal{X} - \mu, \phi_k \rangle \tag{3.7}$$

Further to this decomposition the Karhunen-Loève theorem means we have that the principal components are independent from each other, centred and have variance equal to their associated eigenvalue. That is:

$$\mathbb{E}(\xi_k) = 0 \tag{3.8}$$

$$\text{Var}(\xi_k) = \lambda_k \tag{3.9}$$

$$\mathbb{E}(\xi_k \xi_l) = 0, \text{ for } k \neq l \tag{3.10}$$

3.1.2 Interpretation

As with the multivariate principal components analysis the interpretation of the eigenvectors is often useful in exploratory analysis of data. The functional principal components analysis is of a similar form to the multivariate case and as such the same interpretation of the eigenfunctions is often employed. As such the first eigenfunction $\phi_1(t)$ encapsulates the dominant mode of variation in $\mathcal{X}(t)$ by construction since:

$$\phi_1 = \underset{\|\phi\|=1}{\arg\max}\, \text{Var}\left(\langle \mathcal{X} - \mu, \phi \rangle\right) \tag{3.11}$$

Similarly, the k^{th} eigenfunction is the dominant mode of variation which is orthogonal to the preceding $k-1$ components. As exploring the first few eigenfunctions often gives

a parsimonious way to view the variation in the data. Alike PCA it is often that the modes structure of the eigenfunctions replicates some observed physical process as such the FPCA decomposition is often used widely as a tool for data exploration.

In addition to this we can use the fact that subsequent eigenfunctions capture less and less variation of the data as a form of dimensionality reduction, alike PCA. In this sense we can consider truncating the full representation given in Equation (3.6) to the K leading eigenfunctions which gives an approximation to the full process which we will denote by $\mathcal{X}^K(t)$ where:

$$\mathcal{X}^K(t) = \mu(t) + \sum_{k=1}^{K} \xi_k \phi_k(t) \tag{3.12}$$

The approximation of $\mathcal{X}$ by $\mathcal{X}^K$ converges by:

$$\mathbb{E}\left(\langle \mathcal{X} - \mathcal{X}^K, \mathcal{X} - \mathcal{X}^K \rangle\right) = \sum_{k>K}^{\infty} \lambda_k \to 0 \text{ as } K \to \infty \tag{3.13}$$

As such using the leading principal components for reconstruction has the effect of capturing the main modes of variation of the data and ignoring smaller modes of variation. Choosing the number of principal components is then up to the practitioner as in multivariate PCA, [52]. Ramsay and Silverman discuss in length the comparison of PCA to FPCA including commentary on the optimal choice of number of principal components, [40, Chapter 8]. The practical implementation of FPCA involves then estimating various components. In particular estimation of; the mean function $\mu(t)$, the covariance surface $G(s,t)$, the K eigenfunctions and eigenvalues $\phi_k(t)$, λ_k respectively, and the principal components ξ_k for each realisation of the process $\mathcal{X}$ we observe.

3.2 Principal analysis through conditional expectation

Assuming for now we have a sufficient method for estimating the mean and covariance surfaces which we will denote by $\hat{\mu}(t)$ and $\hat{G}(s,t)$. We discuss in more detail the estimation of these components in Section 3.3. Prior to the introduction of the Principal Analysis through Conditional Expectation (PACE) methodology in [57] FPCA decomposition was restricted due to the need for approximating the integrals in Equations (3.7). As such it was often a requirement that the functional data were observed on a dense regular grid which meant that the principal components could be reliably estimated though some numerical integration scheme, [40, Chapter 8]. This very much restricted the application of the FPCA technique, however Yao et al. introduced the PACE method for over coming such an obstacle using conditional expectations for sparsely observed functional data. In addition to this at the same time the technique accommodates for observation error.

Traditionally Equation (3.7) used for estimating the principal component scores for the i^{th} realisation is approximated through sums. Substituting y_{ij} for $\mathcal{X}(t_{ij})$, $\hat{\mu}(t_{ij})$ for $\mu(t_{ij})$, and $hat\phi_k(t_{ij})$ for $\phi_k(t_{ij})$ we obtain the estimate $\xi_i^S = \sum_1^{J_i} \left(y_{ij} - \hat{\mu}(t_{ij})\right) \hat{\phi}_k(t_{ij}) \left(t_{ij} - t_{i(j-1)}\right)$

[57]. Where y_{ij} is as described in Equation (1.2) and setting $t_{i0} = 0$. However such an estimate breaks for the case that observations are sparse. Similarly such an approximation will be biased when the error processes from Equation (1.2), ε_{ij}, is non-zero. Yao et al. overcomes this by first assuming that the model is as follows:

$$y_{ij} = \chi_i + \varepsilon_{ij} \tag{3.14}$$

$$= \mu(t_{ij}) + \sum_{k=1}^{\infty} \xi_{ik}\phi_k(t_{ij}) + \varepsilon_{ij} \tag{3.15}$$

with ε_{ij} being jointly Gaussian with ξ_{ik}. We also require the noise process satisfies:

$$\mathbb{E}(\varepsilon_{ij}) = 0 \tag{3.16}$$

$$\mathrm{Var}(\varepsilon_{ij}) = \sigma_\varepsilon^2 \tag{3.17}$$

In addition to this the number of measurements of the i^{th} subject is considered random which reflect sparse functional data. Such a description follows naturally from our dataset description given in Equation (1.2) by using the FPCA decomposition structure of $\mathcal{X}$ as discussed in Section 3.1. Following [57] we define the subsequent vector notations:

$$\boldsymbol{Y}_i = (y_{i1}, y_{i2}, \cdots, y_{iJ_i})^\top \tag{3.18}$$

$$\boldsymbol{\phi}_{ik} = (\phi_k(t_{i1}), \phi_k(t_{i2}), \cdots, \phi_k(t_{iJ_i}))^\top \tag{3.19}$$

$$\boldsymbol{\mu}_i = (\mu(t_{i1}), \mu(t_{i2}), \cdots, \mu(t_{iJ_i}))^\top \tag{3.20}$$

$$\boldsymbol{t}_i = (t_{i1}, t_{i2}, \cdots, t_{iJ_i})^\top \tag{3.21}$$

With such a model and assumptions, as stated in [57], the best prediction of the principal component scores for the i^{th} subject is given by:

$$\tilde{\xi}_{ik} = \mathbb{E}(\xi_{ik}|\boldsymbol{Y}_i, \boldsymbol{t}_i) = \lambda_k \boldsymbol{\phi}_{ik}^\top \boldsymbol{\Sigma}_{\boldsymbol{Y}_i}^{-1}(\boldsymbol{Y}_i - \boldsymbol{\mu}_i) \tag{3.22}$$

where $\boldsymbol{\Sigma}_{\boldsymbol{Y}_i} = \mathrm{Cov}(\boldsymbol{Y}_i, \boldsymbol{Y}_i)$. The estimate for the principal component score can then be found by substituting in estimates for the various components in Equation (3.22). That is:

$$\hat{\xi}_{ik} = \hat{\mathbb{E}}(\xi_{ik}|\boldsymbol{Y}_i, \boldsymbol{t}_i) = \hat{\lambda}_k \hat{\boldsymbol{\phi}}_{ik}^\top \hat{\boldsymbol{\Sigma}}_{\boldsymbol{Y}_i}^{-1}(\boldsymbol{Y}_i - \hat{\boldsymbol{\mu}}_i) \tag{3.23}$$

The covariance matrix $\hat{\boldsymbol{\Sigma}}_{\boldsymbol{Y}_i}$ is formed with $(l, m)^{\text{th}}$ element:

$$\left[\hat{\boldsymbol{\Sigma}}_{\boldsymbol{Y}_i}\right]_{lm} = \hat{G}(t_{il}, t_{im}) + \hat{\sigma}_\varepsilon^2 \delta_{lm} \tag{3.24}$$

where $\hat{\sigma}_\varepsilon^2$ is the estimated variance of the noise process. The estimation method for this is discussed in Section 3.3. Yao et al. also provide asymptotic properties of such an estimator along with asymptotic confidence bands where the mean and covariance surfaces are estimated with local linear smoothers, [13].

The conditional expectation technique describe above from [57] alleviates the issue of poor integral approximation from sparsely observed data when the estimated covariance surface is a relatively good fit to the true covariance surface. This is a somewhat better condition as it allows one to pool data from different observed subjects to estimate such a surface and thus the requirement of dense data per subject is relaxed to having dense data from the collection over all subjects. We discuss a particular method for estimating such surfaces in Section 3.3.

3.3 Penalised regression splines

Smoothing models underpin much of FDA. FDA uses the smoothness of observations over a continuous domain to help inform and model observed data. Typically, as described in Section 1.2, data is only observed discretely. Therefore with most FDA methodology there must be a conversion from discretely observed data and the continuous functional variable that generates it. This is particularly the case for our EO data since we have discrete observations specified by our data model given in Equation (1.1) which we assume is generated by observations of continuous functions or surfaces given by our models in Equation (1.2). As such many models for obtaining such a smooth of the data have been studied, such as kernel smoothing, polynomial regression, and local linear smoothing, [40, Chapter 4]. In this section we consider the well studied technique of obtaining smooths of discrete data through penalised spline regression. We will use such a method to estimate the mean and covariance surfaces present in PACE methodology described in Section 3.2.

3.3.1 Basis Splines

One of the components of a penalised spline regression is the basis functions used in the regression. As the name suggests spline regression uses spline functions as the regression basis. Spline functions of order d, which are well documented in the monograph of De Boor, is a piecewise polynomial function of degree $d-1$, [11]. In the case of a spline function of order d, $S : \mathcal{T} \to \mathbb{R}$, over a univariate domain $\mathcal{T} = [a, b] \subset \mathbb{R}$ we have:

$$S : t \mapsto S(t) = \begin{cases} P_0(t) \text{ if } \tau_0 < t \leq \tau_1, \\ P_1(t) \text{ if } \tau_1 < t \leq \tau_2, \\ \vdots \\ P_{m-1}(t) \text{ if } \tau_{m-1} < t \leq \tau_m, \end{cases} \tag{3.25}$$

where $P_i : [\tau_i, \tau_{i+1}] \to \mathbb{R}$ are polynomial functions of degree $d-1$. The vector of points $\boldsymbol{\tau} = (\tau_0, \tau_1, \cdots, \tau_m)$ is known as the knot vector for the spline and must satisfy $a = \tau_0 < \tau_1 < \cdots < \tau_m = b$. By specifying that the piecewise polynomials must share the same derivative order up to a degree we can ensure continuity of relative smoothness over the knot points and the whole spline function. We specify the continuity at each point in our knot vector by the continuity vector $\boldsymbol{r} = (r_0, \cdots, r_m)^\top$ where r_i specifies that P_i and P_{i+1}

share common derivative values at point τ_i for derivatives up to order r_i. The spline type can be specified completely by specifying the knot locations and the continuity vector, [11]. In fact one can extend our definition of the knot vector to incorporate both the knot and continuity vector into one vector, known as the extended knot vector, which will completely specify the spline type. We define the extended knot vector as the vector of knot points which repeats the i^{th} knot vector exactly $n - r_i$ times. That is:

$$(\tau_0, \cdots, \tau_0, \tau_1, \cdots, \tau_1, \cdots, \tau_{m-1}, \cdots, \tau_{m-1}, \tau_m \cdots, \tau_m)$$

We denote the spline functions of order d with extended knot vector by $S_{d,\boldsymbol{\tau}}$.

The Basis splines are more commonly referred to as B-splines, [29]. B-splines are basis functions for splines of the same order defined over the same knots. They are typically defined recursively, [29, 11]. The classic algorithm for the recursive construction is known as the Cox-de Boor recursion formula, [11], and is given as follows. Given a knot vector $(\tau_0, \cdots, \tau_0, \tau_1, \cdots, \tau_1, \cdots, \tau_{m-1}, \cdots, \tau_{m-1}, \tau_m, \cdots, \tau_m)^\top$ the B-spline of order 1 is given by:

$$B_{i,1}(t) = \begin{cases} 1, \text{ for } \tau_i \leq t < \tau_{i+1} \\ 0, \text{ otherwise.} \end{cases} \tag{3.26}$$

The higher order B-splines are defined by recursion as:

$$B_{i,q+1}(t) = w_{i,p}(t) B_{i,q}(t) + [1 - w_{i+1,q}(t)] B_{i+1,q}(t) \tag{3.27}$$

where $w_{i,q}$ is a weighting for the i^{th} B-spline of order d given by:

$$w_{i,q}(t) = \begin{cases} \frac{x - \tau_i}{\tau_{i+q} - \tau_i}, \text{ for } \tau_{i+q} \neq \tau_i \\ 0, \text{ otherwise.} \end{cases} \tag{3.28}$$

A B-spline basis system of size Q can then be considered by choosing the extended knot vector $\boldsymbol{\tau}$ and specifying the order, d, of the B-spline functions, and is given by the collection:

$$\{B^{\boldsymbol{\tau}}_{d,q}(t)\}_{q=1}^{Q} \tag{3.29}$$

where Q is the number of basis functions to use in the system, $\boldsymbol{\tau}$ is the extended knot vector, and $B^{\boldsymbol{\tau}}_{d,q}$ is the q^{th} B-spline of order d defined by Equation (3.27) for our knot vector $\boldsymbol{\tau}$. Figure 3.1 shows the first 7 B-spline functions of order 4 with equally spaced knots over the domain $[0, 1]$.

3.3.2 Regression splines

As discussed in Section 3.2 the PACE methodology requires estimation of both the mean function, $\mu(t)$, and covariance surface $G(s, t)$. Estimating such functions is a problem due to their infinite dimensional nature. A well studied and effective method for representing such functions is the use of a basis function expansion, [40]. That is representing the

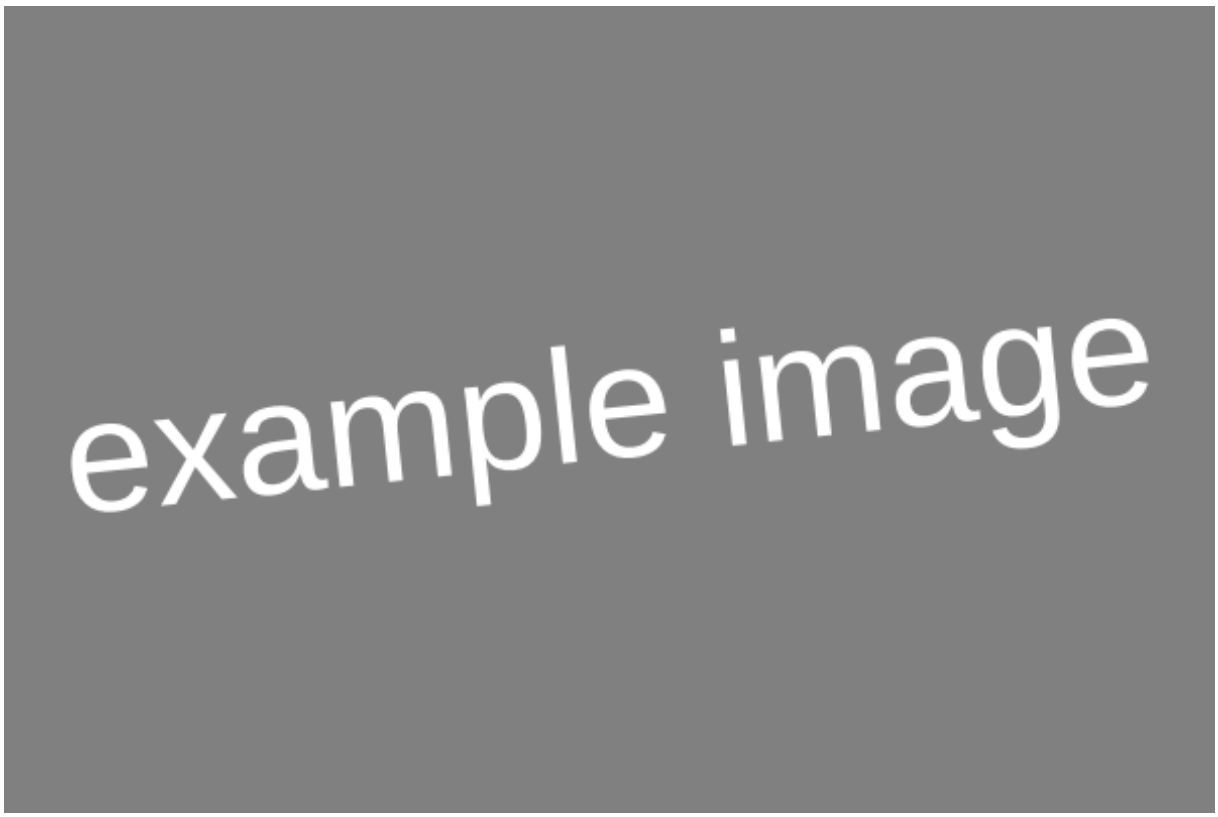

Fig. 3.1 First seven B-spline functions of order four with equally spaced interior knots over the domain $[0, 1]$. The vertical dotted lines indicate the knot positions.

target surface using a linear combination of known basis functions. In this work we will utilise the B-spline basis function as discussed in Section3.3.1. The B-spline system is exceptionally popular due to its ease of computation and ability to reconstruct many surfaces, [11]. Such ease of computation makes it feasible to not only create large basis systems but also alleviates many fitting procedures as we can re-evaluate the basis system at various points with ease. Such properties are very useful when using such a basis for regression models. Common basis systems include the Fourier, Monomial, and Polynomial basis systems, [40]. In the following we present the approach for estimating an arbitrary realisation of our functional random variable $\chi(t)_i$ over domain $\mathcal{T}$ and discuss how we extend the same concept to a two dimensional surface over $\mathcal{T} \times \mathcal{T}$ in Section3.3.2.

As such we assume that our function can be represented using an order d B-spline basis system with knot vector $\boldsymbol{\tau}$:

$$\chi(t)_i = \sum_{q=1}^{Q} c_q B_{d,q}^{\boldsymbol{\tau}}(t) \tag{3.30}$$

$$= \boldsymbol{c}^{\intercal} \boldsymbol{B}_d^{\boldsymbol{\tau}}(t) \tag{3.31}$$

$$\tag{3.32}$$

where $\boldsymbol{c} = (c_1, \cdots, c_K)^{\intercal}$, $\boldsymbol{B}_d^{\boldsymbol{\tau}}(t) = \intercal\Big(B_{d,1}^{\boldsymbol{\tau}}(t), B_{d,2}^{\boldsymbol{\tau}}(t), \cdots, B_{d,Q}^{\boldsymbol{\tau}}(t)\Big)$, and Q is the dimension of the expansion. An example of such a basis expansion is given in Figure 3.2. From

this we can clearly see how the function χ_i is broken down into a finitely many constituent parts of scaled known basis functions. If such basis functions have nice properties such as simplicity to compute then such a representation for f given by Equation (3.31) can be extremely useful since most problems can be reduced to problems involving the finite dimensional vector $\boldsymbol{c} \in \mathbb{R}^Q$.

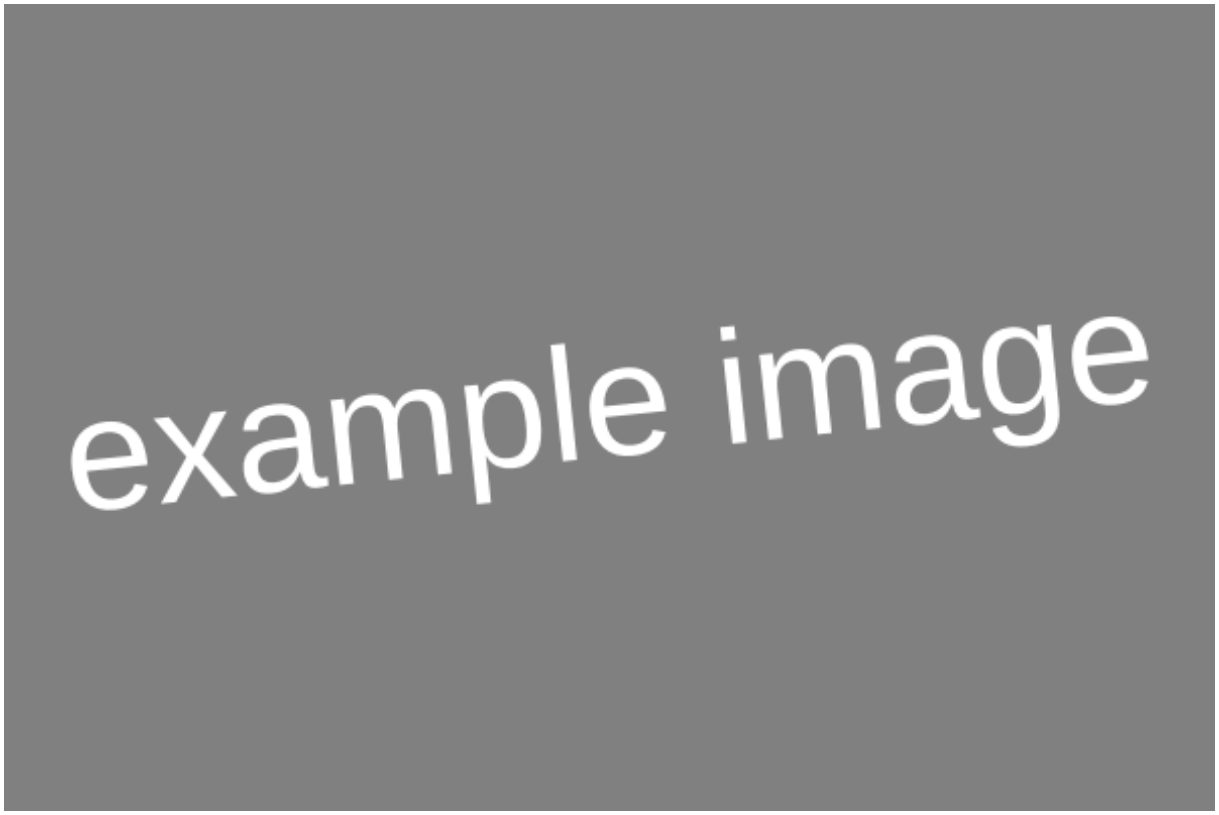

Fig. 3.2 Example B-spline basis expansion of known function with basis functions shown for clarity.

Our representation of χ_i using a basis system then becomes the problem of choosing the coefficients $\boldsymbol{c}^\intercal$ using only our set of observations of $\boldsymbol{Y}_i$ which are observed with error. The most common method for fitting a basis system to discretely observed data is by choosing the coefficients of the expansion c_q given in Equation 3.31 by minimising the criterion:

$$\text{SSE}_{\boldsymbol{Y}_i}(\boldsymbol{c}) = \|\boldsymbol{Y}_i - \boldsymbol{B}\boldsymbol{c}^\intercal\|^2 \tag{3.33}$$

where $\boldsymbol{B} = (\boldsymbol{B}_d^\tau(t_{i1}), \boldsymbol{B}_d^\tau(t_{i2}), \cdots, \boldsymbol{B}_d^\tau(t_{iJ_i}))^\intercal$ is the $J_i \times Q$ matrix of the basis system evaluated at observed time points corresponding to the J_i length observation vector $\boldsymbol{Y}_i$. Minimising such a criterion is given by, [6]:

$$\hat{\boldsymbol{c}} = \left(\boldsymbol{B}^\intercal \boldsymbol{B}\right)^{-1} \boldsymbol{B}^\intercal \boldsymbol{Y}_i \tag{3.34}$$

The simple least squares approximation is a well studied and standard approach. See [6] for a through introduction to the concept. Such a methodology is often suitable for situations where our error process $\varepsilon(t)$ is a white noise process. Such a process for the noise is often unrealistic; as such a simple adjustment to the least squares criterion in

Equation 3.33 can be used to allow for correlation among the observation errors:

$$\text{SSE}_{\boldsymbol{Y}_i,\boldsymbol{W}}(\boldsymbol{c}) = \|\boldsymbol{W}^{\frac{1}{2}}\left(\boldsymbol{Y}_i - \boldsymbol{B}\boldsymbol{c}^\intercal\right)\|^2 \tag{3.35}$$

where $\boldsymbol{W}$ is a weighting matrix for the observations. Ideally the matrix will be the inverse of the variance-covariance matrix of the observations. Minimising the adjusted criterion is given by, [6]:

$$\hat{\boldsymbol{c}} = \left(\boldsymbol{B}^\intercal\boldsymbol{W}\boldsymbol{B}\right)^{-1}\boldsymbol{B}^\intercal\boldsymbol{W}\boldsymbol{y} \tag{3.36}$$

The estimate with least squares fitting can then be substituting $\hat{\boldsymbol{c}}$ for the $\boldsymbol{c}$ in Equation3.31, [6]. That is:

$$\hat{\chi}_i(t) = \hat{\boldsymbol{c}}^\intercal\boldsymbol{B}_d^\tau(t) \tag{3.37}$$

The selection of the knot vector is well studied and the classical choice is to choose a knot vector where knots are located at the sampling points, [11].

An issue with the classical least squares fitting using a basis system expansion is the choice of number of basis functions, [40]. Although we are constrained to choose Q to be less than or equal to the number of observations, J_i, since more than J_i basis functions would results in Equation 3.36 being ill defined as the matrix $\boldsymbol{B}$ cannot have linearly independent columns. However, we still have the choice to choose Q between 1 and J_i. Exactly which value for Q to choose is unknown and results in the classical problem of bias variance trade off in the estimator. A large number of basis functions reduces bias in the estimator $\hat{\chi}_i(t)$, but the variance of this estimator may be unacceptably high. Similarity a lower number of basis functions will result in high bias of the estimator but low variance. The bias-variance trade off is well studied and there is a vast literature on the methodology of choosing the number of basis functions, however there is no gold standard and often the choice is made in an ad hoc fashion, [40]. Such an issue motivates modifying the fitting criterion which determines $\hat{\boldsymbol{c}}$ in Equation (3.36).

Penalties

Ideally we want to penalise estimators which have high variance, that occur naturally when we have a large number of basis functions, but keep bias low. The naive choice of just reducing the number of basis functions, known as regression splines, fails in this respect, [43]. One such approach to do this is to reduce the number of basis functions in conjunction with a penalty, known as penalised regression splines. Such an approach was first used in [38] who used such a formulation on ill posed inverse problems. [43] discuss various other spline smoothing techniques as well as the penalised regression splines.

Penalised regression spline models adjust the fitting criterion in Equation (3.36) to:

$$\text{PSSE}_{\boldsymbol{Y}_i,\boldsymbol{W},\lambda}(\boldsymbol{c}) = \|\boldsymbol{W}^{\frac{1}{2}}\left(\boldsymbol{Y}_i - \boldsymbol{B}\boldsymbol{c}\right)\|^2 + \omega\boldsymbol{c}^\intercal\boldsymbol{P}\boldsymbol{c} \tag{3.38}$$

where $\boldsymbol{P}$ is formed with $(l,m)^{\text{th}}$ element $[\boldsymbol{P}]_{lm} = \langle L\left(\boldsymbol{B}_l\right), L\left(\boldsymbol{B}_m\right)\rangle$ and ω is a parameter which controls the regularisation trade off. L is some linear differential operator. Typically

one chooses L to be the required smoothness of the target function and examples include simple first or second derivatives, [43].

Analytically minimising the PSSE criterion in Equation (3.38) can be found via:

$$\hat{\boldsymbol{c}} = \left(\boldsymbol{B}^\intercal \boldsymbol{W} \boldsymbol{B} + \omega \boldsymbol{P}\right)^{-1} \boldsymbol{B}^\intercal \boldsymbol{W} \boldsymbol{Y}_i \tag{3.39}$$

Essentially such a penalisation term determines that there should be a trade off between the bias which corresponds to the first term in Equation (3.38) and the variance which is the second term. This trade off is controlled by the regularisation parameter ω. The advantage of this method is that we can now let Q, our number of basis functions, be large without worrying of over fitting as the penalty term in Equation (3.38) will penalise functions with high variability in terms of the differential operator L.

The choice of differential operator is a well studied problem also. A common choice is the first or second order differential, denoted by D^1 and D^2 respectively, as this specifies a reasonable level of smoothness in the target function, [43]. However, often more complex terms are used to facilitate known properties of the target functions, such a letting L be the harmonic acceleration operator which forces a periodic form of the target functions. More care must be taken when extending the linear differential operator to higher dimensions which is discussed in Section 3.3.2. Additionally, in the case of B-spline basis system these penalty matrices are typically evaluated using a form of numerical integration, [40].

Considering a penalised for of regression splines moves our problem of selecting Q to choosing our regularisation parameter, ω. Such a parameter influences the strictness with which we expect our target function to be smooth as defined by the operator L. Choosing such a parameter is a problem that is present not only in spline smoothing but other penalised regression approaches, [33]. A popular method for choosing such a parameter is the Generalised Cross Validation (GCV). GCV, introduced by Wahba,, is a well studied method which has good asymptotic properties as J_i, the number of observations tends to infinity, [50, 49]. GCV chooses λ as the minimiser of the GCV criterion $V(\omega)$ which is given by:

$$V\left(\omega\right) = \frac{J_i^{-1} \| \left(\boldsymbol{I} - \boldsymbol{A}\right) \boldsymbol{Y}_i \|^2}{\left[J_i^{-1} \mathrm{tr}\left(\boldsymbol{I} - \boldsymbol{A}\right)\right]^2} \tag{3.40}$$

where $\boldsymbol{A}$ is the influence matrix defined by:

$$\boldsymbol{A} = \boldsymbol{B}\left(\boldsymbol{B}^\intercal \boldsymbol{W} \boldsymbol{B} + \omega \boldsymbol{P}\right)^{-1} \boldsymbol{B}^\intercal \boldsymbol{W} \tag{3.41}$$

The GCV method can then be minimised for ω using a numerical minimisation routing. For large J_i it is known that the GCV criterion performs well in recovering a regularisation parameter which minimises variance while maintaining low bias in the reconstruction of the target function, [49]. For the case of low J_i the GCV method may not be reliable as such method to extend the GCV criterion have been considered. The modified GCV criterion, which adds a further modifier to the denominator in Equation (3.40) by multiplying the trace of the influence matrix by a factor, [10]. The modified GCV approach effectively

increases the cost associated with each effective parameter in the curve which reduces choosing ω which under smooths the data, [10]. A similar but separate approach to adjusting the GCV is robust GCV, introduced by Lukas, which uses a weighted sum of the GCV function with a term which penalises ω values that are close to zero, [33]. The performance of such methods are discussed in [34].

Choosing a basis system, a criterion to choose the regularisation parameter and a differential operator then fully specified the penalised regression spline approach. In the case of one dimensional functions the procedure applies as above. As such we can estimate our mean function $\mu(t)$ through the use of a penalised spline regression where our observation points for the mean function are the pooled mean across subject of the union of observed time points for all curves. However for multiple dimensions, particularly the case when we wish to smooth the covariance surface, we must make some adjustments to the penalty. These are discussed in Section 3.3.2.

Extension to higher dimensions

There are two issues when extending the penalised regression spline to higher dimensions; extending the basis system and extending the penalty specification. To alleviate the first we must specify a basis system which can cover multiple dimensions. In fact there are many such systems, [50]. One such popular approach when we have regular data for FDA is using a tensor product B-spline system, [56]. Consider a two dimensional surface$\sigma(s,t)$ which we represent by the tensor product spline given by:

$$\sigma(s,t) = \sum_{1 \leq q_1, q_2 \leq \bar{Q}} c_{q_1,q_2} \boldsymbol{B}_{d_1}^{\boldsymbol{\tau}_1}(s) \boldsymbol{B}_{d_2}^{\boldsymbol{\tau}_2}(t) \tag{3.42}$$

where $\boldsymbol{B}_{d_i}^{\boldsymbol{\tau}_i}$ is the B-spline basis system for the i^{th} dimension for $i = 1, 2$. For notational simplicity we assume the dimension of each marginal basis system is the same, $\bar{Q}$ however this need not be the case. $\boldsymbol{C} \in \mathbb{R}^{\bar{Q} \times \bar{Q}}$ is a coefficient matrix to be determined. Equation (3.42) can be written more succinctly using a Kronecker product as:

$$\sigma(s,t) = \bar{\boldsymbol{B}}^{\mathsf{T}}(s,t) \operatorname{Vec}(\boldsymbol{C}) \tag{3.43}$$

where $\bar{\boldsymbol{B}}(s,t) = \boldsymbol{B}_{d_2}^{\boldsymbol{\tau}_2}(t) \otimes \boldsymbol{B}_{d_1}^{\boldsymbol{\tau}_1}(s)$ and $\operatorname{Vec}(\cdot)$ is an operator which stacks the columns of a matrix into a vector. We use the $\bar{\cdot}$ notation to make explicit that this basis is over multiple dimensions.

The same methods now follow as in the non penalised univariate case with this Kronecker basis system, [56]. However, we must still adjust the penalty matrix in Equation (3.39) to account for smoothness across multiple dimensions.

Using the tensor product basis system as described above one might consider specifying that the smoothness of the surface in smooth in both dimensions. Indeed, one such approach to extending the penalty specification which was introduced by Wood is to consider setting penalties on the marginal basis separately and to combine them by a weighted sum, [54]. Such an approach known as tensor product penalties is well studied in

the linear generalised additive model setting, [53]. A two dimensional penalty matrix $\bar{\boldsymbol{P}}$ may be described as follows:

$$\bar{\boldsymbol{P}} = \omega_1 \boldsymbol{P}_1 \otimes \boldsymbol{I}_2 + \omega_2 \boldsymbol{I}_1 \otimes \boldsymbol{P}_2 \tag{3.44}$$

where $\boldsymbol{P}_i$ is marginal penalty over a single basis dimension as described in Equation (3.38), I_i is the identity matrix of dimension of the i^{th} dimension basis, and $omega_i$ is the marginal regularisation parameter for $i = 1, 2$. The properties of such a smoothness penalty are discussed in detail in [54] with the main points being such a penalty is both scale invariant and low rank. In addition [55] studies the use of such a penalty for the case of unevenly distributed data. The additional complication is we now have multiple smoothness parameters ω_i, one for each dimension of the surface to be smoothed. In this case the GCV methodology can still be applied but now minimisation occurs with respect to the vector $\boldsymbol{\omega}$. Implementation details of such can be found in [53].

With an extension to multiple dimensions we can now use the above approach to estimate our covariance surface, denoted by $\hat{G}(s,t)$, for use in PACE methodology, [57]. The discrete observations for the covariance surface to be smoothed are gathered by pooling individual observed covariances from across subjects, which is discussed in detail in both [57, 56]. Xiao provides asymptotic properties of such an approach to the covariance surface of independent functional data which are on par to the asymptotic results of other smoothers used in [57] for the PACE methodology, [56].

3.4 Functional time series

As discussed in Section 1.1 EO data is often both spatially and temporally correlated. This two types of correlation is often considered separately. An area in FDA which has considered a similar case where functional data is observed and observations are correlated is functional time series, [2]. Typically, functional observations are naturally indexed by some time of observation and correlation may occur between observations. Hence we may build up a time series of functional observations. Functional time series models are some of the first in the FDA literature to start to consider correlated functional observations. Although they limit themselves to temporal correlation many of the ideas can be considered for extensions to higher dimension correlation and so we discuss a few of the more popular methodologies in this section.

We focus on a technique introduced by Hyndman and Shang in [24] to forecast functional time series. Such a method is of interest as it expands methodology on how to use existing forecasting techniques in a functional setting. In particular [24] uses the FPCA decomposition described in Section 3.1 to decompose functional observations and then uses independent forecasting of each principal component scores using standard multivariate techniques.

[23] suggests to assume the principal component scores, ξ_{ik} follow independent univariate time series. Then, conditioning on the observed data Y given in Equation (1.1) and the

set of principal components $\boldsymbol{\phi}(t) = (\phi_1(t), \phi_2(t), \cdots, \phi_K(t))$ they obtain the h-step ahead forecast of $y_{i+h|i}(t)$ as:

$$\hat{y}_{i+h|i} = \mathbb{E}\left(y_{i+h}(t)|\boldsymbol{Y}, \boldsymbol{\phi}\right) = \hat{\mu}(t) + \sum_{k=1}^{K} \hat{\xi}_{i+h|i,k}\phi_k(t) \tag{3.45}$$

where $\hat{\xi}_{i+h|i,k}$ denotes the h-step ahead forecast of the k^{th} principal component score. The method for which $\hat{\xi}_{i+h|i,k}$ is obtained can be any univariate time series method. Such methods are extremely well studied and discussed in the monograph [21]. Hyndman and Booth highlight the case the forecast is relatively insensitive to the choice of number of components in the principal decomposition provided it is sufficiently large. The variance of such a method can also easily be obtained through the sum of the component variances. The component variance of the forecast principal component scores are generally readily available from many time series models, [21]. The above forecasting methodology initially described in [23] used normal FPCA procedure with outliers weighted to zero, however this was reconsidered in [24] to include a geometric weighting to the principal components to allow for changes in the function over time.

Such a methodology motivates the construction of the CPACE model described in Chapter 5 for correlated functional data by considering the case where the principal components scores obey univariate correlated models not just time series. To describe some of these such models we use the concept of a Gaussian Process. We give background to this in the following section.

3.5 Gaussian process regression

The above section of functional time series shows there is scope for placing a model on the principal component scores to allow for correlation among functional observations. The natural progression to such work is to consider what options are available when we have more complex correlation structure or higher dimensional domain. For example, in the case of EO data discussed in Section 1.1 we have functional observations over a spatial domain, $\mathcal{S}$ indexed by some coordinate $\boldsymbol{s} \in \mathcal{S}$. For this the univariate time series methods discussed in [24] are not suitable and we look to Gaussian processes as one possible solution to model principal component scores which are indexed by space. A such we discuss the basic concept of a Gaussian process in the following.

A real valued stochastic process is a collection of real random variables defined on the same probability space $(\Omega, \mathcal{F}, \mathcal{P})$ where Ω is a sample space, $\mathcal{F}$ is a σ-algebra, and $\mathcal{P}$ is a probability measure; and the random variables, indexed by some set $\mathcal{S}$ are all real valued. More details of such constructions can be found in [5]. A stochastic process can then be written as the collection:

$$\{\xi(\boldsymbol{s}, w)|\boldsymbol{s} \in \mathcal{S}\}$$

where $w \in \Omega$. A sample function of the stochastic process is the mapping, for a point $w \in \Omega$:

$$\xi(\cdot, w) : \mathcal{S} \to \mathbb{R}$$

A Gaussian process is a stochastic process which is parametrised by a mean function $m : \mathcal{S} \to \mathbb{R}$ where $m(\boldsymbol{s}) = \mathbb{E}(\xi(\boldsymbol{x}))$ and its covariance function:

$$k : \mathcal{S}^2 \to \mathbb{R}$$
$$k : \boldsymbol{s} \mapsto \mathrm{Cov}(\xi(\boldsymbol{s}), \xi(\boldsymbol{s}))$$

where for any finite collection of points, $\boldsymbol{s}_1, \boldsymbol{s}_2, \cdots, \boldsymbol{s}_n \in \mathcal{S}$, the joint distribution of $\boldsymbol{\xi}_n = (\xi(\boldsymbol{s}_1), \xi(\boldsymbol{s}_2, \cdots, \xi(\boldsymbol{s}_n))^\intercal$ is a multivariate normal distribution with mean vector $\boldsymbol{m}_n = (m(\boldsymbol{s}_1), m(\boldsymbol{s}_2), \cdots, m(\boldsymbol{s}_n))^\intercal$ and covariance matrix $\boldsymbol{K}_n$ whose $(l, m)^{\text{th}}$ entry is given by $k(\boldsymbol{s}_l, \boldsymbol{s}_m)$, [46]. As such, Gaussian processes are a natural way of defining a prior distribution over spaces of functions, which are the parameter spaces for Bayesian non linear regression models. In this work we will denote such a Gaussian process by $\mathcal{GP}$ and write:

$$\xi(\cdot) \sim \mathcal{GP}(m(\cdot), k(\cdot, \cdot)) \tag{3.46}$$

One aspect of Gaussian process regression models is that under Gaussian assumptions they have a nice closed form for prediction. Let $S = \{\boldsymbol{s}_1, \boldsymbol{s}_2, \cdots, \boldsymbol{s}_n\}$ denote the design matrix of the regression, and $\boldsymbol{\xi}$ denote the corresponding target vector. Then conditioning the joint Gaussian prior distribution on the observations gives, [51]:

$$\boldsymbol{\xi}_* | S_*, S, \boldsymbol{\xi} \sim \mathcal{N}\left(K(S_*, S)K(S, S)^{-1}\boldsymbol{\xi}, K(S_*, S_*) - K(S_*, S)K(S, S)^{-1}K(S, S_*)\right) \tag{3.47}$$

where $K(\cdot, \cdot)$ is the covariance matrix formed by evaluating the covariance function $K(\cdot, \cdot)$ at all pairs of inputs. This can be extended easily to noisy observations by adjusting the observed covariance $K(S, S)$ to include a diagonal component which is the effect of model observation error. See [51] for details.

One key aspect of the Gaussian process is the covariance function $k(\cdot, \cdot)$. The covariance function characterises various smoothness properties such as the sample path continuity and its differentiability. As such the choice of $k(\cdot, \cdot)$ heavily influences the prediction mean and covariance as described in Equation (3.47). There are various common forms of the covariance function but all must have the intrinsic property of being non-negative definite. The covariance function is of such importance in Gaussian process modelling and spatial statistics that it has been widely studied. See [51, Chapter 4] for a detailed introduction to various covariance functions. We expand on Section 1.3 to briefly introduce our form of covariance function which we will consider throughout this work.

Of the many different covariance functions employed in Gaussian processes stationary covariance functions are most commonly employed due to their simplicity and ease of construction, [8]. One such commonly used covariance function is the Matèrn covariance

function which is given by:

$$C_\nu(d) = \sigma^2 \frac{2^{1-\nu}}{\Gamma(\nu)} \left(\sqrt{2\nu} d\right)^\nu K_\nu \left(\sqrt{2\nu} d\right) \tag{3.48}$$

where Γ is the gamma function, K_ν is the modified Bessel function of the second kind, ν is a shape parameter of the kernel, and d is the possibly anisotropic separation between two vectors $\boldsymbol{s}, \boldsymbol{s}'$, [1]. The covariance kernel $k(\boldsymbol{s}, \boldsymbol{s}')$ is then simply $C_\nu(d(\boldsymbol{s}, \boldsymbol{s}'))$.

The issue with stationary covariance forms is that they are often quite restrictive in the sense that the correlation structure cannot vary across the domain. For example, this might be a too restrictive assumption in the case of climate data where correlation structure might be quite different in different parts of the globe. One particular way to extend the stationary Matèrn kernel to be non-stationary is proposed in [39]. Paciorek and Schervish propose a method to knit together multiple stationary correlation functions such that the resultant function is non-stationary.

They provide a form of non-stationary covariance function $k^{NS}(\cdot, \cdot)$ from stationary covariance function $k^S(\cdot, \cdot)$ as follows, [39]:

$$k^{NS}(\boldsymbol{s}, \boldsymbol{s}') = |\Sigma_{\boldsymbol{s}}|^{\frac{1}{4}} |\Sigma_{\boldsymbol{s}'}|^{\frac{1}{4}} \left|\frac{\Sigma_{\boldsymbol{s}} + \Sigma_{\boldsymbol{s}'}}{2}\right|^{-\frac{1}{2}} k^S(Q(\boldsymbol{s}, \boldsymbol{s}')) \tag{3.49}$$

where $Q(\boldsymbol{s}, \boldsymbol{s}') = (\boldsymbol{s} - \boldsymbol{s}')^\intercal \left(\frac{\Sigma_{\boldsymbol{s}} + \Sigma_{\boldsymbol{s}'}}{2}\right)^{-1} (\boldsymbol{s} - \boldsymbol{s}')$ and $\Sigma_{\boldsymbol{s}} = \Sigma(\boldsymbol{s})$ is the covariance matrix of the Gaussian kernel centred at $\boldsymbol{s}$. How $\Sigma_{\boldsymbol{s}}$ varies across the domain specifies how non-stationary the full covariance kernel is.

With almost all covariance functions and especially non-stationary covariances there are typically hyper parameters which must be estimated from the data. For example in the Matèrn covariance we have the shape parameter ν and any length scale parameters defined in the distance function $d(\cdot, \cdot)$. These are typically estimated though maximum likelihood estimation, [51], however fully Bayesian estimation can also be achieved through some Markov Chain Monte Carlo (MCMC) scheme, [39].

Chapter 4

Dynamic functional time series modelling

Chapter 5

Correlated principal analysis through conditional expectation

Chapter 6

Application of CPACE model

Chapter 7

Implementation of CPACE model

Chapter 8

Conclusions and further work

References

[1] Abramowitz, M. and Stegun, I. A., editors (2013). *Handbook of mathematical functions: with formulas, graphs, and mathematical tables*. Number 1 in Dover books on mathematics. Dover Publ, New York, NY.

[2] Aguilera, A. M., Ocaña, F. A., and Valderrama, M. J. (1999). Forecasting time series by functional PCA. Discussion of several weighted approaches. *Computational Statistics*, 14(3):443–467.

[3] Aschbacher, J. and Milagro-Pérez, M. P. (2012). The European Earth monitoring (GMES) programme: Status and perspectives. *Remote Sensing of Environment*, 120:3–8.

[4] Aston, J. A. D., Pigoli, D., and Tavakoli, S. (2017). Tests for separability in nonparametric covariance operators of random surfaces. *The Annals of Statistics*, 45(4):1431–1461.

[5] Billingsley, P. (1995). *Probability and Measure*. Wiley. Google-Books-ID: z39jQgAACAAJ.

[6] Björck, A. (1996). *Numerical methods for least squares problems*. SIAM, Philadelphia.

[7] Cressie, N. and Huang, H.-c. (1999). Classes of Nonseparable, Spatio-temporal Stationary Covariance Functions. *Journal of the American Statistical Association*, 94:1330–1340.

[8] Cressie, N. A. C. (2010). *Statistics for spatial data*. Wiley, New York. OCLC: 1039155476.

[9] Cressie, N. A. C. and Wikle, C. K. (2011). *Statistics for spatio-temporal data*. Number 1 in Wiley series in probability and statistics. Wiley, Hoboken, N.J.

[10] Cummins, D. J., Filloon, T. G., and Nychka, D. (2001). Confidence Intervals for Nonparametric Curve Estimates: Toward More Uniform Pointwise Coverage. *Journal of the American Statistical Association*, 96(453):233–246. Publisher: [American Statistical Association, Taylor & Francis, Ltd.].

[11] De Boor, C. (2001). *A practical guide to splines: with 32 figures*. Number v. 27 in Applied mathematical sciences. Springer, New York, rev. ed edition.

[12] Deb, S. and Tsay, R. S. (2017). Spatio-temporal models with space-time interaction and their applications to air pollution data. *arXiv:1801.00211 [stat]*. arXiv: 1801.00211.

[13] Fan, J., Gijbels, I., Hu, T.-C., and Huang, L.-S. (1996). A STUDY OF VARIABLE BANDWIDTH SELECTION FOR LOCAL POLYNOMIAL REGRESSION. *Statistica Sinica*, 6(1):113–127. Publisher: Institute of Statistical Science, Academia Sinica.

[14] Ferraty, F. and Vieu, P. (2006). *Nonparametric Functional Data Analysis*. Springer Science+Business Media, Inc., New York. OCLC: 318296135.

[15] Fuentes, M. (2006). Testing for separability of spatial–temporal covariance functions. *Journal of Statistical Planning and Inference*, 136(2):447–466.

[16] George, B. and Aban, I. (2015). Selecting a Separable Parametric Spatiotemporal Covariance Structure for Longitudinal Imaging Data. *Statistics in medicine*, 34(1):145–161.

[17] Gneiting, T. (2002). Nonseparable, Stationary Covariance Functions for Space-Time Data. *Journal of the American Statistical Association*, 97(458):590–600.

[18] Higdon, D. (2002). Space and Space-Time Modeling using Process Convolutions. In Anderson, C. W., Barnett, V., Chatwin, P. C., and El-Shaarawi, A. H., editors, *Quantitative Methods for Current Environmental Issues*, pages 37–56, London. Springer.

[19] Hooker, G., Roberts, S., and Shang, Lin, H. (2015). Maximal autocorrelation factors for function-valued spatial/temporal data. In *Weber, T., McPhee, M.J. and Anderssen, R.S. (eds) MODSIM2015, 21st International Congress on Modelling and Simulation*. Modelling and Simulation Society of Australia and New Zealand.

[20] Hurrell, J. W., Holland, M. M., Gent, P. R., Ghan, S., Kay, J. E., Kushner, P. J., Lamarque, J.-F., Large, W. G., Lawrence, D., Lindsay, K., Lipscomb, W. H., Long, M. C., Mahowald, N., Marsh, D. R., Neale, R. B., Rasch, P., Vavrus, S., Vertenstein, M., Bader, D., Collins, W. D., Hack, J. J., Kiehl, J., and Marshall, S. (2013). The Community Earth System Model: A Framework for Collaborative Research. *Bulletin of the American Meteorological Society*, 94(9):1339–1360. Publisher: American Meteorological Society Section: Bulletin of the American Meteorological Society.

[21] Hyndman, R. J. and Athanasopoulos, G. (2018). *Forecasting: principles and practice*. OTexts. Google-Books-ID: _bBhDwAAQBAJ.

[22] Hyndman, R. J. and Booth, H. (2008). Stochastic population forecasts using functional data models for mortality, fertility and migration. *International Journal of Forecasting*, 24(3):323–342.

[23] Hyndman, R. J. and Shahid Ullah, M. (2007). Robust forecasting of mortality and fertility rates: A functional data approach. *Computational Statistics & Data Analysis*, 51(10):4942–4956.

[24] Hyndman, R. J. and Shang, H. L. (2009). Forecasting functional time series. *Journal of the Korean Statistical Society*, page 13.

[25] Iaco, S. D., Myers, D. E., and Posa, D. (2002). Nonseparable Space-Time Covariance Models: Some Parametric Families. *Mathematical Geology*, 34(1):23–42.

[26] Karhunen, K. (1946). Zur Spektraltheorie stochastischer Prozesse. *Ann. Acad. Sci. Finnicae, Ser. A*, 1:34.

[27] Kay, J. E., Deser, C., Phillips, A. S., Mai, A., Hannay, C., Strand, G., Arblaster, J. M., Bates, S. C., Danabasoglu, G., Edwards, J. C., Holland, M. M., Kushner, P. J., Lamarque, J.-F., Lawrence, D. M., Lindsay, K., Middleton, A., Munoz, E., Neale, R. B., Oleson, K. W., Polvani, L. M., and Vertenstein, M. (2015). The Community Earth System Model (CESM) large ensemble project: a community resource for studying climate change in the presence of internal climate variability. *Bulletin of the American Meteorological Society*, 96(8):1333–1349. Publisher: American Meteorological Society.

[28] Khabbazan, S., Vermunt, P., Steele-Dunne, S., Ratering Arntz, L., Marinetti, C., van der Valk, D., Iannini, L., Molijn, R., Westerdijk, K., and van der Sande, C. (2019). Crop Monitoring Using Sentinel-1 Data: A Case Study from The Netherlands. *Remote Sensing*, 11(16):1887. Number: 16 Publisher: Multidisciplinary Digital Publishing Institute.

[29] Knott, G. D. (2000). *Interpolating Cubic Splines*. Number 1 in Progress in Computer Science and Applied Logic. Birkhäuser Basel.

[30] Lindgren, F., Rue, H., and Lindström, J. (2011). An explicit link between Gaussian fields and Gaussian Markov random fields: the stochastic partial differential equation approach. *Journal of the Royal Statistical Society: Series B (Statistical Methodology)*, 73(4):423–498. _eprint: https://rss.onlinelibrary.wiley.com/doi/pdf/10.1111/j.1467-9868.2011.00777.x.

[31] Liu, C., Ray, S., Hooker, G., and Friedl, M. (2012). Functional factor analysis for periodic remote sensing data. *The Annals of Applied Statistics*, 6(2):601–624.

[32] Loève, M. (1946). Fonctions aléatoires à décomposition orthogonale exponentielle. *La Revue Scientifique*, 84:159–162.

[33] Lukas, M. A. (2006). Robust generalized cross-validation for choosing the regularization parameter. *Inverse Problems*, 22(5):1883–1902. Publisher: IOP Publishing.

[34] Lukas, M. A., Hoog, F. R. D., and Anderssen, R. S. (2012). Performance of Robust GCV and Modified GCV for Spline Smoothing. *Scandinavian Journal of Statistics*, 39(1):97–115. _eprint: https://onlinelibrary.wiley.com/doi/pdf/10.1111/j.1467-9469.2011.00736.x.

[35] Militino, A. F., Ugarte, M. D., and Pérez-Goya, U. (2018). An Introduction to the Spatio-Temporal Analysis of Satellite Remote Sensing Data for Geostatisticians. In Daya Sagar, B., Cheng, Q., and Agterberg, F., editors, *Handbook of Mathematical Geosciences: Fifty Years of IAMG*, pages 239–253. Springer International Publishing, Cham.

[36] Mitchell, M. W., Genton, M. G., and Gumpertz, M. L. (2006). A likelihood ratio test for separability of covariances. *Journal of Multivariate Analysis*, 97(5):1025–1043.

[37] Muro, J., Canty, M., Conradsen, K., Hüttich, C., Nielsen, A. A., Skriver, H., Remy, F., Strauch, A., Thonfeld, F., and Menz, G. (2016). Short-Term Change Detection in Wetlands Using Sentinel-1 Time Series. *Remote Sensing*, 8(10):795. Number: 10 Publisher: Multidisciplinary Digital Publishing Institute.

[38] O'Sullivan, F. (1986). A Statistical Perspective on Ill-Posed Inverse Problems. *Statistical Science*, 1(4):502–518. Publisher: Institute of Mathematical Statistics.

[39] Paciorek, C. J. and Schervish, M. J. (2006). Spatial Modelling Using a New Class of Nonstationary Covariance Functions. *Environmetrics*, 17(5):483–506.

[40] Ramsay, J. O. and Silverman, B. W. (2010). *Functional data analysis*. Springer Science+Business Media, New York (N.Y.).

[41] Raspini, F., Bianchini, S., Ciampalini, A., Del Soldato, M., Solari, L., Novali, F., Del Conte, S., Rucci, A., Ferretti, A., and Casagli, N. (2018). Continuous, semi-automatic monitoring of ground deformation using Sentinel-1 satellites. *Scientific Reports*, 8(1):7253. Number: 1 Publisher: Nature Publishing Group.

[42] Rossi, R. E., Dungan, J. L., and Beck, L. R. (1994). Kriging in the shadows: Geostatistical interpolation for remote sensing. *Remote Sensing of Environment*, 49(1):32–40.

[43] Ruppert, D., Wand, M. P., and Carroll, R. J. (2003). *Semiparametric Regression*. Cambridge Series in Statistical and Probabilistic Mathematics. Cambridge University Press, Cambridge.

[44] Sampson, P. D. and Guttorp, P. (1992). Nonparametric Estimation of Nonstationary Spatial Covariance Structure. *Journal of the American Statistical Association*, 87(417):108–119. Publisher: [American Statistical Association, Taylor & Francis, Ltd.].

[45] Schmidt, A. M. and Guttorp, P. (2020). Flexible spatial covariance functions. *Spatial Statistics*, 37:100416.

[46] Shi, J. Q. and Choi, T. (2011). *Gaussian Process Regression Analysis for Functional Data*. CRC Press. Google-Books-ID: DkgdN6dRAicC.

[47] Stein, M. L. (1999). *Interpolation of Spatial Data Some Theory for Kriging*. OCLC: 1184292315.

[48] Wahba, G. (1977). Practical Approximate Solutions to Linear Operator Equations when the Data are Noisy. *SIAM Journal on Numerical Analysis*, 14(4):651–667. Publisher: Society for Industrial and Applied Mathematics.

[49] Wahba, G. (1985). A Comparison of GCV and GML for Choosing the Smoothing Parameter in the Generalized Spline Smoothing Problem. *The Annals of Statistics*, 13(4):1378–1402. Publisher: Institute of Mathematical Statistics.

[50] Wahba, G. (1990). *Spline Models for Observational Data*. CBMS-NSF Regional Conference Series in Applied Mathematics. Society for Industrial and Applied Mathematics.

[51] Williams, C. K. and Rasmussen, C. E. (2006). *Gaussian processes for machine learning*, volume 2. MIT press Cambridge, MA.

[52] Wold, S., Esbensen, K., and Geladi, P. (1987). Principal component analysis. *Chemometrics and intelligent laboratory systems*, 2(1-3):37–52. Publisher: Elsevier.

[53] Wood, S. N. (2006a). *Generalized Additive Models: An Introduction with R*. CRC Press LLC, Philadelphia, PA, UNITED STATES.

[54] Wood, S. N. (2006b). Low-rank scale-invariant tensor product smooths for generalized additive mixed models. *Biometrics*, 62(4):1025–1036.

[55] Wood, S. N. (2017). P-splines with derivative based penalties and tensor product smoothing of unevenly distributed data. *Statistics and Computing*, 27(4):985–989. arXiv: 1605.02446.

[56] Xiao, L. (2020). Asymptotic properties of penalized splines for functional data. *Bernoulli*, 26(4):2847–2875. Publisher: Bernoulli Society for Mathematical Statistics and Probability.

[57] Yao, F., Müller, H.-G., and Wang, J.-L. (2005). Functional Data Analysis for Sparse Longitudinal Data. *Journal of the American Statistical Association*, 100(470):577–590. Publisher: [American Statistical Association, Taylor & Francis, Ltd.].

[58] Zhang, C., Li, W., and Travis, D. J. (2009). Restoration of clouded pixels in multispectral remotely sensed imagery with cokriging. *International Journal of Remote Sensing*, 30(9):2173–2195. Publisher: Taylor & Francis _eprint: https://doi.org/10.1080/01431160802549294.